Journal of Materials Chemistry B

ROYAL SOCIETY OF CHEMISTRY

REVIEW

View Article Online
View Journal | View Issue



Cite this: *J. Mater. Chem. B*, 2024, **12**, 1404

# Magnetic two-dimensional nanocomposites for multimodal antitumor therapy: a recent review

Ying Yuan,† Bo Chen,† Luping Song, Xingxing An, Qinrui Zhang, Hao Lu, Chang Ming Li* and Chunxian Guo *

Magnetic two-dimensional nanocomposites (M2D NCs) that synergistically combine magnetic nanomedicine and 2D nanomaterials have emerged in multimodal antitumor therapy, attracting great interest in materials science and biomedical engineering. This review provides a summary of the recent advances of M2D NCs and their multimodal antitumor applications. We first introduce the design and fabrication of M2D NCs, followed by discussing new types of M2D NCs that have been recently reported. Then, a detailed analysis and discussions about the different types of M2D NCs are presented based on the structural categories of 2D NMs, including 2D graphene, transition metal dichalcogenides (TMDs), transition metal carbides/nitrides/carbonitrides (MXenes), black phosphorus (BP), layered double hydroxides (LDHs), metal organic frameworks (MOFs), covalent organic frameworks (COFs) and other 2D nanomaterials. In particular, we focus on the synthesis strategies, magnetic or optical responsive performance, and the versatile antitumor applications, which include magnetic hyperthermia therapy (MHT), photothermal therapy (PTT), photodynamic therapy (PDT), drug delivery, immunotherapy and multimodal imaging. We conclude the review by proposing future developments with an emphasis on the mass production and biodegradation mechanism of the M2D NCs. This work is expected to provide a comprehensive overview to researchers and engineers who are interested in such a research field and promote the clinical translation of M2D NCs in practical applications.

Received 7th October 2023,
Accepted 21st December 2023

DOI: 10.1039/d3tb02333h

rsc.li/materials-b



*Institute of Materials Science and Devices, School of Materials Science and Engineering, Suzhou University of Science and Technology, 99 Xuefu Road, Suzhou, 215009, Jiangsu, P. R. China. E-mail: ecmli@usts.edu.cn, cxguo@usts.edu.cn*

† These authors contributed equally to this work.

**Ying Yuan**

*Ying Yuan is currently pursuing her Master's degree from the Suzhou University of Science and Technology under the guidance of Prof. Chang Ming Li and Associate Prof. Bo Chen. She received her Bachelor's degree in Environmental Sciences from Bengbu University in 2021. Her current research interest is the construction of two-dimensional magnetic nanocomposites and investigation into their antitumor and antibacterial application.*

**Bo Chen**

*Bo Chen is working as an Associate Professor in the School of Materials Science and Engineering, Suzhou University of Science and Technology. He has received his PhD from Southeast University in 2018, under the guidance of Prof. Ning Gu (academician of Chinese Academy of Sciences). He has earned Natural Science Fund for Excellent Youth Scholars of Jiangsu Province and other awards in the field of biomedical nanotechnologies. His research interests focus on the design and construction of high performance magnetic/chiral/optical/sonic-driven nanoplatform for diverse biomedical applications (**https://clxy.usts.edu.cn/info/1113/1229.htm**).*

# 1. Introduction

Tumor treatment has attracted increasing attention in the field of biomedical research due to the complicated and refractory nature of malignant tumors. Conventional approaches, such as chemotherapy and radiotherapy, have struggled to overcome tumor tolerance and metastasis while causing detrimental effects on normal tissues or organs during the therapeutic process.[1] Recently, emerging antitumor technologies, including magnetic hyperthermia therapy (MHT), photothermal therapy (PTT), photodynamic therapy (PDT), drug delivery and multimodal imaging have attracted great attention.[2,3] However, most of the therapeutic modalities alone appear to be insufficient in adequately addressing the problems, *e.g.*, tumor tolerance, metastasis and off-target effects.[4,5] Multimodal antitumor approaches that combine different therapeutic modalities are regarded as promising strategies for tumor treatment. A desired multimodal therapeutic agent should deliver precise targeting to tumors, prominent inhibition of tumor growth and metastasis, accurate imaging localization, excellent biocompatibility and minimal adverse effects.[6] The burgeoning nanomaterials have led to recent advances in multimodal antitumor nanoagents.[6,7] Theranostic nanoagents with unique properties, including good physiological stability, tailored degradation metabolism routes and optical/thermal/magnetic stimulus-responsive behaviors, have significantly boosted the development of multimodal antitumor therapy.[8]

Two-dimensional nanomaterials (2D NMs) with a unique planar nanostructure exhibit promising characteristics such as high specific surface area, tailored surface and interface properties and tunable band gap.[9] Its 2D nanostructure has rich active sites and can enhance specific physicochemical activities for desired interaction with biosystems, thus holding promise in the antitumor field.[10–12] In recent years, a variety of 2D NMs including graphene oxide (GO), transition metal dichalcogenides (TMDs),[13] 2D transition metal carbides/nitrides/carbonitrides (MXenes),[14] phosphorene (BPNS),[15] layered double hydroxides (LDHs),[9] 2D metal–organic frameworks (MOFs)[16] and 2D covalent-organic frameworks (COFs),[17] have been explored in tumor diagnostics and therapy. For example, BPNS shows remarkable fluorescence and near-infrared (NIR) imaging capabilities and 2D $MoS_2$ has been employed in two-photon fluorescence (TFP) bioimaging in tumor diagnosis,[18] while MXenes have demonstrated excellent contrast in X-ray computed tomography (CT) imaging.[19] As for tumor treatment, multimodal antitumor therapy comprising PTT and PDT is realized based on 2D NMs-induced cell apoptosis or necrosis.[20,21] BPNSs have been developed as a theranostic system, incorporating doxorubicin (DOX) for chemotherapy and cyanine for NIR imaging, while functionalizing with folic acid to achieve targeted delivery.[22] 2D $MoSe_2$ exhibits multimodal PTT and PDT outcomes, which are significantly higher compared to Au nanoparticles (NPs).[23] Therefore, increasing attention is being paid to 2D NMs for their promising multimodal antitumor therapy.

Magnetic nanomaterials (MNMs) encompass nanoscale dopants or alloys of magnetic metals such as Fe, Co, Ni, Mn, Gd, magnetic metal oxides, and transition metal ferrites.[24] Due to their high magnetic behavior and good biocompatibility, MNMs have been investigated for various biomedical applications,[25] which include magnetic resonance imaging (MRI),[26] magneto hyperthermia therapy (MHT),[27,28] stem cell labeling/tracking, immunotherapies under magnetic guidance, chemodynamic therapy (CDT) and magneto-responsive drug delivery.[29,30] Iron-based magnetic NPs have been granted clinical approval for use in MRI and iron supplements.[31] In our previous work, a magnetic hydrogel complex was designed and fabricated by loading DOX into an iron-based nanodrug of Ferumoxytol, followed by encapsulation in chitosan, and exhibited pH- and temperature-dependent drug release behavior.[32]

**Chang Ming Li**

*Chang Ming Li is working as a Doctoral supervisor at the School of Materials Science and Engineering, Suzhou University of Science and Technology. He received his PhD and MS degrees in Physical Chemistry at Wuhan University. He received his BS degree in Polymer Physics from the University of Science and Technology of China. He was awarded as a member of the European Academy of Science, Fellow of the American Institute for Medical and Biological Engineering, and Fellow of the Royal Society of Chemistry. His research areas include functional materials, nanoscience and nanomaterials, green energies, and sensors.*

**Chunxian Guo**

*Chunxian Guo is working in the School of Materials Science and Engineering, Suzhou University of Science and Technology. He was awarded with the National High Level Talent Plan for Young Talents, and served as the director of Jiangsu Province Biochemical Sensing and Chip Technology Engineering Laboratory. He received his PhD from the School of Chemical and Biomedical Engineering, Nanyang Technological University in Singapore. His research interests focus on the regulation of physicochemical properties of materials, the building of high-efficiency chemical energy and ultrasensitive sensors, and investigation into applications in the fields of chemical energy and sensor analysis.*

Moreover, MNMs have been found to show exotic intrinsic enzyme-like activities, promoting numerous novel paradigms for tumor therapy.[33–36] For instance, the pyrite nanozyme proposed by Yan *et al.*, exhibits ultrahigh peroxidase (POD)-like and glutathione oxidase-like activities, constituting a self-cascade platform capable of generating abundant •OH and depleting glutathione, and demonstrating more than 3000-fold increase of POD catalytic efficiency than that of natural horseradish peroxidase (HRP).[33] Nevertheless, although they show magnetic and enzyme-like activities, plain MNMs are not suitable for multimodal antitumor therapy because of their relatively low surface area, poor optical and thermal responsive behaviors. Recent efforts have been focused on the design of MNMs-based nanocomposites for improved multimodal antitumor performance.

Very recently, magnetic 2D nanocomposites (M2D NCs) that synergistically combine 2D NMs and MNMs have attracted extensive attention because of their promising multimodal antitumor applications. They have shown unique physicochemical properties, including optical, magnetic, catalytic, and other intriguing characteristics.[37] For example, a magnetic BPNS/$MnO_2$ nanocomposite was designed as an intelligent self-propelled theranostic platform, showcasing specific tumor-targeting properties, simultaneous pH/redox-responsive MRI performance, and also pH dependent drug release behavior.[38] A magnetic reduced graphene oxide (RGO)-iron oxide (IO) nanocomposite was developed as a $T_2$-MRI guided PTT therapy platform.[39] Recent advances have been achieved for the design and fabrication of M2D NCs and their multimodal antitumor applications. Increasingly more researchers and engineers are beginning to get involved in such a research field. However, there still lacks a timely and comprehensive review about this research field.

In this review, we present an overview of the recent advances in M2D NCs and their nanoagents for multimodal antitumor implementation (Fig. 1). Advantages of the synergistic combination of 2D NMs and MNMs into M2D NCs are firstly introduced. Then, we present the design and material fabrication of M2D NCs, including MNMs assembled on 2D NMs, 2D NMs assembled on MNMs, and *in situ* synthesis. Next, we summarize and discuss the multimodal antitumor applications of M2D NCs that are mainly based on 2D graphene and its derivatives, transition metal dichalcogenides (TMDs), transition metal carbides/nitrides/carbonitrides (MXenes), black phosphorus (BPs),

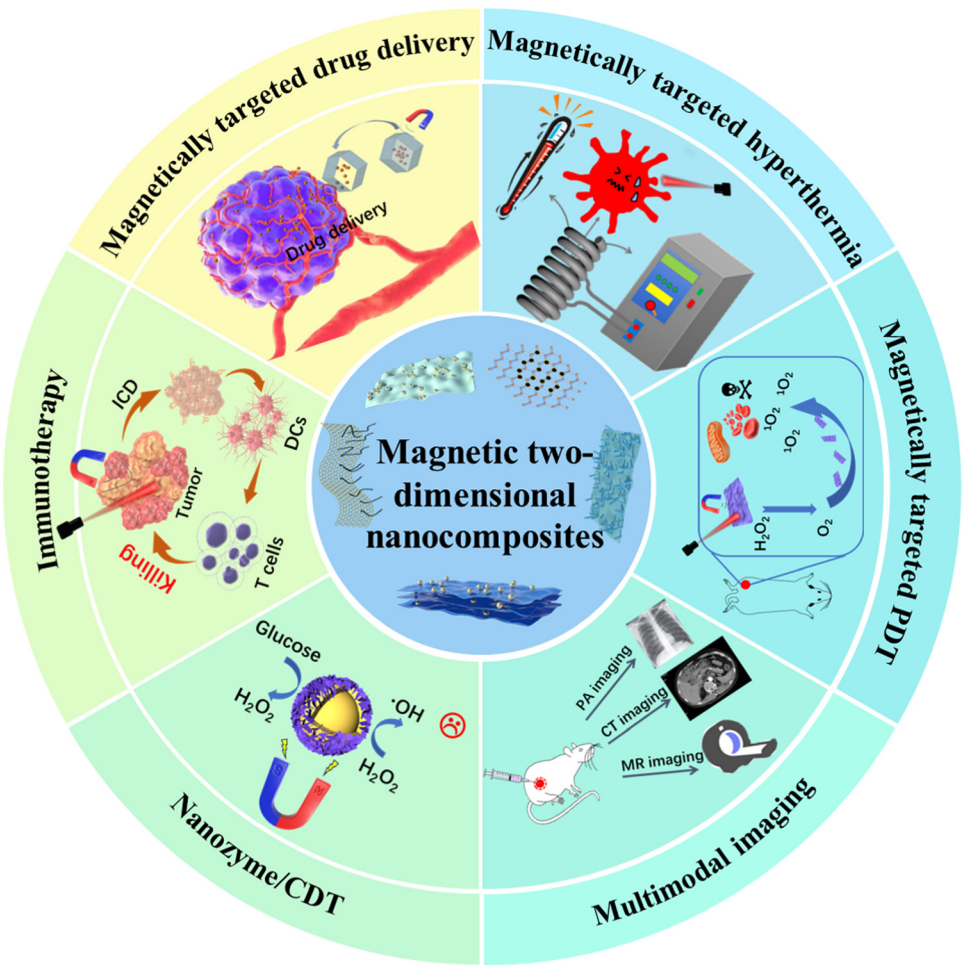


Fig. 1 Schematic illustration of the recent advances of magnetic 2D nanocomposites (M2D NCs) and their multimodal tumor therapy and diagnosis.

 

layered double hydroxides (LDHs), metal–organic frameworks (MOFs) and covalent-organic frameworks (COFs). In particular, a detailed analysis is conducted on the multimodal applications, including MHT, PTT, PDT, drug delivery, immunotherapy and multimodal imaging. This review concludes by proposing the future development of such a research field with emphasis on the challenges and clinical prospect, including the material customization, exploration of structure-performance relationships, scaling up of the material fabrication, meeting medicinal demand, and elucidating the biodegradation mechanism.

# 2. Advantages of the combination of 2D NMs and MNMs into M2D NCs

## 2.1 Advantages and challenges of 2D NMs in antitumor treatment

Despite the successful fabrication of various 2D NMs through diverse approaches and their extensive application in the field of antitumor theranostics, there are still numerous obstacles that hinder their further applications, primarily including interior stability in physiological environments, poor hydrophilicity, non-negligible biotoxicity, off-target manipulation issues, insufficient photoconversion efficacy and others. From a thermodynamic perspective, the 2D structure faces challenges in maintaining a persistent stable state due to its high surface energy resulting from a significant proportion of exposed unsaturated atoms. Thus, it is not suitable for long-term utilization *in vivo*.[40] Secondly, the majority of 2D NMs exhibit a tendency to aggregation in physiological media, potentially causing damage to normal tissues or organs.[41] Additionally, the release of heavy metal ions from the 2D NMs during decomposition *in vivo* may exceed the tolerance levels of human body, and result in detrimental irreversible impacts on healthy regions. Herein, BPNS is used as an example to discuss the advantages and disadvantages of 2D NMs' metabolic stability. On the one hand, BPNS rapidly decomposes after *in vivo* administration, and is eventually transformed into phosphates or phosphonates that can be reabsorbed and reused by the body.[42] This non-toxic metabolic pathway reduces concerns about potential long-term risks. On the other hand, the short metabolic cycle in the physiological environment severely limits its effectiveness on tumor treatment. Upon exposure to air and water, BPNS rapidly collapses, resulting in a significant reduction of the antitumor outcomes. Thirdly, phototherapy alone by virtue of 2D NMs is generally insufficient for complete tumor eradication. Unfortunately, the current PTT regimen is plagued by challenges such as non-uniform heat distribution and suboptimal hyperthermia outcomes, which significantly impede its clinical translation expansion, particularly for deep-seated metastatic tumors.[43,44] As for PDT, the majority of 2D photosensitizers encounter shortcomings involving high dark toxicity, short blood circulation time, hypoxia microenvironment, and other factors, which ultimately lead to unsatisfactory outcomes.[45] Furthermore, it has been demonstrated that single PDT or PTT alone is inadequate for complete tumor eradication.[43] Based on the aforementioned analysis, there is an urgent need for the development of novel 2D nanocomposites with a multifaceted therapeutic approach to overcome these challenges and significantly enhance tumor treatment efficacy.

## 2.2 Advantages and challenges of plain MNMs in antitumor applications

Akin to 2D NMs, the clinical implementation of MNMs is hindered by their inadequate treatment regimes, despite the establishment of various MNM types. It should be noted that several challenges remain unresolved, such as the poor delivery efficiency and uncertainties regarding the balance between the dosage security and therapeutic/diagnostic performance.[85,86] For instance, ferritin-modified MNMs have shown promise as an anticancer nano-vector, but further understanding is needed regarding their impact on inflammation, apoptotic body formation, reactive oxygen species (ROS) production and chromosome aggregation.[87] Moreover, improving the colloidal stability and preventing the carrier media aggregation or precipitation in plasma and tissues are crucial for reducing the acute and long-term toxicity.[88,89] Moreover, it has been observed that exposure to ACMF activates the heat-tolerance pathway in melanoma cells treated with MNMs, indicating that the rapid establishment of thermotolerance alone is insufficient for effective tumor ablation.[90] Overall, in order to address the aforementioned critical clinical issues, it is imperative to explore innovative MNMs that exhibit enhanced safety profiles and multifaceted antitumor capabilities. This necessitates expanding the composition and structure of MNMs, with a focus on pioneering breakthroughs in clinical practice.

## 2.3 Synergetic M2D NCs for multimodal tumor therapy

As summarized in Table 1, it can be clearly observed that advanced magnetic 2D nanocomposites (M2D NCs) present a promising approach to integrate their respective advantages and tackle critical challenges faced by both materials. In fact, the practical implementation of the M2D NCs strategy has demonstrated its efficacy in achieving optimal tumor therapy and imaging Firstly, it is noteworthy that both 2D NMs and MNMs possess flexible surface activities, which enable the convenient construction of diverse nanocomposite structures for specific antitumor scenarios. Well-ordered magnetic nanocomposites prolong degradation and metabolism, ensuring durable stability *in vivo* to maximize their therapeutic effects. Secondly, the integration of individual phototherapy, magnetotherapy and related imaging properties into one platform through the establishment of M2D NCs significantly enhances the convenience and versatility in practice compared to mono materials. It is expected that neither single 2D NMs nor single MNMs can match the optical/magneto responsiveness of M2D NCs based on current studies. Moreover, by employing various modification measures and coupling groups, M2D NCs can serve as stimuli-responsive drug carriers. A variety of

Table 1 Summary of the advantages of M2D NCs compared to single therapy of 2D NMs in tumor treatment

| 2D NMs | M2D NCs | Advantages of M2D NCs |
|---|---|---|
| GO | GO-IONP-PEG-DOX[46] | Magnetically targeted DOX delivery, localized PTT guided by magnetic field |
| GO | FeMn-GO[47] | Efficient pH-responsive drug releasing performance and redox-triggered $T_1$-weighted MRI |
| GQD | GQD-MMSNs-DOX[48] | pH-responsive DOX delivery and significant synergistic MHT and PTT |
| GQD | HMNS/$SiO_2$/GQD[49] | Magneto-mechanical and PTT synergetic therapy |
| GQD | $MnFe_2O_4$@$SiO_2$@GQDs/DAU[50] | pH-responsive DAU delivery and fluorescence resonance energy transfer (FRET) system-enhanced apoptosis |
| GO | $MnO_2$@Pd@PPy/GO[51] | Strong PTT performance, pH-responsive enzymatic and enhanced MRI performance |
| GQD | Cur/GQDs-$Fe_3O_4$-FA[52] | pH-responsive Cur delivery and magnetic targeting delivery |
| $WS_2$ | $WS_2$-IO@MS-PEG-DOX[53] | Triple modal fluorescence, MR and X-ray CT imaging guided PTT |
| $WS_2$ | $WS_2$:$Gd^{3+}$-PEG[54] | Strong NIR absorbance and X-ray attenuation ability enables contrasts in PA imaging and CT |
| $MoS_2$ | $MoS_2$/$Fe_3O_4$[55] | Magnetic targeted PTT, dual-modal probe for $T_2$-weighted MR and PAT imaging |
| $MoS_2$ | $MoS_2$-IO-PEG[56] | Triple modal PET, PAT, and MRI guided PTT |
| $MoS_2$ | Mo@Fe-ICG/Pt[57] | Enhanced antitumor efficacy of combined PTT, PDT, and chemotherapy triggered by a single 808 nm NIR laser |
| $Ti_3C_2$ | MnOx/$Ti_3C_2$[58] | Unique tumor microenvironment-responsive $T_1$-weighted MRI and PTT performance |
| $Ta_4C_3$ | MnOx/$Ta_4C_3$[59] | TME-responsive $T_1$-weighted MRI and enhanced PTT |
| $Ti_3C_2$ | $Ti_3C_2$-IONP-MXene[60] | Enhanced PTT combined with efficient $T_2$-MRI |
| $Ta_4C_3$ | $Ta_4C_3$-IONP-SPs[61] | Superior PTT effect combined with dual modal CT imaging and $T_2$-MRI |
| $Ti_3C_2$ | $Ti_3C_2$-$Fe_3O_4$@$SiO_2$-FA[62] | pH-dependent drug release and controlled magnetic therapy |
| $Ti_3C_2$ | FTC[63] | Superior PTT performance and enhanced MRI |
| BPNSs | BPs@Au@$Fe_3O_4$[64] | Strong tumor inhibition efficacy, MRI-monitored visualized synergistic PDT and PTT |
| BPNSs | $R^e$-$MnO_2$-$F^f$BP[65] | MR/FL dual-modal imaging, continuous local $O_2$ supply to overcome hypoxia for enhanced PDT |
| BPNSs | BPN/$MnO_2$/DOX[38] | pH and redox-responsive MRI, synergistically enhanced PTT, PDT, and chemotherapy |
| BPNSs | MUCNPs@BPNS-Ce6[66] | Activated PTT and PDT under a single irradiation light of 808 nm |
| BPNSs | BPNS-Arg-GOx@$MnO_2$ (BAGM)[67] | Reinforced synergistic PTT/starvation therapy/NO gas therapy triggered by the cascade reaction |
| BPNSs | RGD-BPNS@SMFN[15] | Target-deliverable PTT–PDT self-synergetic therapy, temperature-dependent catalase (CAT)-like behavior |
| BPQDs | BPQDs@DOX@ss-$Fe_3O_4$@C-EGFR NPs[68] | pH/NIR/GSH-responsive DOX delivery combined with augmented PTT effect |
| MgAl-LDH | LDH-Gd/Au[69] | pH-responsive DOX delivery, dual modal CT and $T_1$-MR imaging performance |
| MgAl-LDH | Mn-LDH[70] | Targeted MR imaging |
| MgAl-LDH | MnFe-LDH-MTX[71] | Strong magnetic responsibility and pH-responsive MTX delivery |
| MnAl-LDH | Mn-LDH-siRNA[72] | Effective anticancer drug/gene delivery and $T_1$-MRI for theranostics |
| CaAl-LDH | LDHs/$Fe_3O_4$@dextran/DOX[73] | pH-responsive DOX delivery and magnetic controlled drug release |
| MgAl-LDH | FA-BSA/$Fe_3O_4$@LDH/5-Fu[74] | Efficient magnetic responsiveness, pH-responsive 5-Fu delivery |
| ZIF-8 | $Fe_3O_4$/ZIF-8-$Au_{25}$[75] | Magnetically targeted PDT/PTT triggered by single 808 nm laser |
| Mn-MOF | $Mn_3O_4$-PEG@C&A[76] | Glutathione consumption and $O_2$ supply by CAT-like activity of $Mn_3O_4$ for enhancing PDT efficacy |
| Co-Fc MOF | Co-Fc@GOx[77] | Cascade enzymatic/Fenton catalytic, versatile and effective drug delivery |
| ZIF-8 | Fe@ZIF-8@GOx[78] | Magnetic enhanced cellular uptake and cascade enzymatic/Fenton catalytic ROS generation |
| COF | $Fe_3O_4$@COF-DhaTph[79] | Significant PTT and PDT effect, triple-modal MRI/PAI/NIRI |
| COF | COF-Au–$MnO_2$-HA[80] | Highly efficient cascade reactions and $T_1$-weighted MRI |
| COF | $Fe_3O_4$@COF-BSA-FA[81] | Highly efficient targeted drug delivery with excellent PTT and magnetic performance |
| BNNs | Pd@OH-BNNSs/DOX[82] | pH/GSH/NIR-responsive delivery and synergetic CDT and PTT |
| $FePSe_3$ | $FePSe_3$@APP@CCM[83] | Multifunctional synergetic combination of MRI and PAI, PTT and immunotherapy |
| g-$C_3N_4$ | $C_3N_4$-Fe-TPP NF/MB[84] | Superior PDT performance and effective $T_1$-weighted MRI |

hydrophobic chemotherapeutic drugs, including camptothecin (CPT),[39,91] DOX,[92–94] 1,3-bis(2-chloroethyl)-1-nitrosourea (BCNU) ellagic acid[95] and β-lapachone[96] have been successfully conjugated covalently or non-covalently adsorbed onto of M2D NCs with considerable capacity. These conjugates exhibit well-controlled release behavior in response to external stimuli, such as laser and magnetic field.[97] Rational surface modification can further enhance the targeting ability and stability of M2D NCs, while simultaneously mitigating their side effects. This approach aligns well with clinical demands. Lastly, a rational and comprehensive nanocomposite may give rise to more extraordinary biological machinery that directly impacts the therapeutic and imaging performance. Notably, innovative therapeutic modalities such as cascade-augmented nanozymes and self-advanced intelligent nanoreactors have been established in advanced M2D NCs.[98–101] Collectively, it is evident that the construction of M2D NCs significantly leverages the inherent properties of both materials to address challenging issues, and shows great potential as a tumoricidal therapy option that has garnered significant interest, boosting research on novel theranostic modalities.

 

# 3. Design and material fabrication of multifunctional M2D NCs

As illustrated in Fig. 2, a variety of M2D NCs have been developed in recent years for antitumor applications. Material fabrication strategies for the 2D NMs can be categorized into top-down and bottom-up routes, which mainly involve hydrothermal/solvothermal methods,[102,103] chemical vapor deposition (CVD),[104,105] liquid phase exfoliation,[106,107] mechanical stripping,[108,109] and electrospinning methods.[110,111] Meanwhile, commonly employed methods for the synthesis of MNMs include co-precipitation, microemulsion and thermal decomposition.[110,112,113] Both 2D NMs and MNMs synthesized in their original forms offer fascinating modification flexibility, enabling convenient tailoring of the multitudinous M2D NCs structure.[114,115] To date, numerous strategies have been developed for the construction of advanced M2D NCs,[41,101,116] which can be broadly categorized into two approaches, namely, post-synthetic surface modification and *in situ* growth of one on the other.[91,112] The former involves assembly of the two materials, while the latter typically results in a more stable structure through *in situ* growth. Hereinafter, we classify various composite structures based on the aforementioned pathways as post-synthetic modification type, including MNM@2D NM composites and 2D NM@MNM composites, and *in situ* synthesis method.

### 3.1 Synthesis of MNMs on the 2D NMs composite (MNMs@2D NMs)

In this approach, pre-synthesized 2D NMs serve as a robust scaffold, offering abundant binding sites for the growth or modification of MNMs (Fig. 3A). Generally, 2D NMs are initially prepared through either bottom-up or top-down processes, and subsequently functionalized with MNMs *via* covalent or non-covalent linkages. Covalent bonding is commonly achieved through radical reactions, cycloaddition reactions, or by introducing oxygen-containing functional groups. Non-covalent modifications are typically achieved through hydrophobic and van der Waals forces, electrostatic interactions, hydrogen bonding, and π–π stacking interactions.[112] For instance, Akshaya *et al.* reported a facile one-pot hydrothermal synthesis method for preparing polymer-stabilized IONP-graphene drug carriers.[117] Ma *et al.* synthesized a functionalized graphene oxide (GO)–iron oxide nanocomposite by anchoring paramagnetic iron oxide nanoparticles (IONP) and chemotherapeutic drug DOX onto the surface of graphene, then wrapping it with polyethylene glycol (PEG).[46] The as-obtained GO-IONP-PEG-DOX serves as a multifunctional cancer treatment platform that combines magnetic targeting drug delivery, chemotherapy, and MHT. Shadie *et al.* synthesized a GO/Co nanocomposite by using GO as the carrier material and assembling cobalt NPs with a size of around 15 nm on the surface of GO.[118] This approach is well-suited for loading MNMs of small size onto 2D NMs with a substantial surface area, representing a form of surface passivation strategy. The presence of abundant magnetic particles covering the 2D NMs mitigates rapid decomposition. Furthermore, this method facilitates the anchoring of other molecules or functional materials, thereby extending its applicability.

### 3.2 Synthesis of 2D NMs on the MNMs composite (2D NMs@MNMs)

In this approach, pre-synthesized MNMs serve as the scaffold for loading or bonding with 2D NMs (Fig. 3B). It is important to note that these MNMs must be functionalized with capping agents or active groups before 2D NMs can grow or anchor onto their surface through covalent linkage, hydrogen bonding, electrostatic interactions, π–π stacking, and other physicochemical mechanisms.[112] Yao *et al.* fabricated a novel magnetic nanocarrier based on graphene oxide (GO) through the following steps: magnetic mesoporous $Fe_3O_4$@$SiO_2$ NPs were first prepared *via* solvothermal method and encapsulated with DOX in the silica shell, followed by grafting of amino-functionalized graphene quantum dots (GQDs) onto the outermost layer of the $Fe_3O_4$@$SiO_2$ NPs to form the nanocomposite (Fig. 3A).[48] Analogously, Zhang *et al.* developed pH/NIR/GSH-responsive BPQD-$Fe_3O_4$@C nanocarriers through disulfide cross-linking (ss-$Fe_3O_4$@C NCs) using black phosphorus quantum dots (BPQDs) as a capping agent in a one-step method, similar to the aforementioned technology. This approach allows for easy manipulation to obtain M2D NCs.[68] This approach is suitable for loading small-sized 2D NMs, such as QDs and NPs, onto MNMs with a larger diameter. As MNMs occupy the core of the nanocomposite, this material consistently exhibits superior

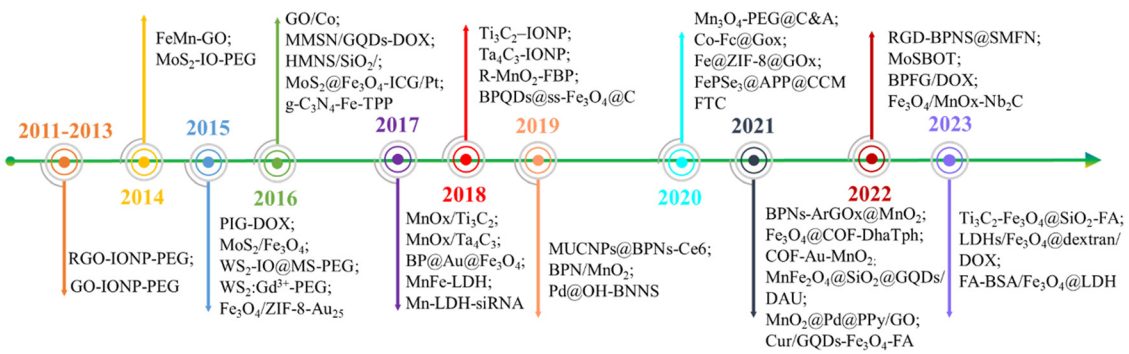


Fig. 2 A brief timeline of the development of M2D NCs in the applications of antitumor field.

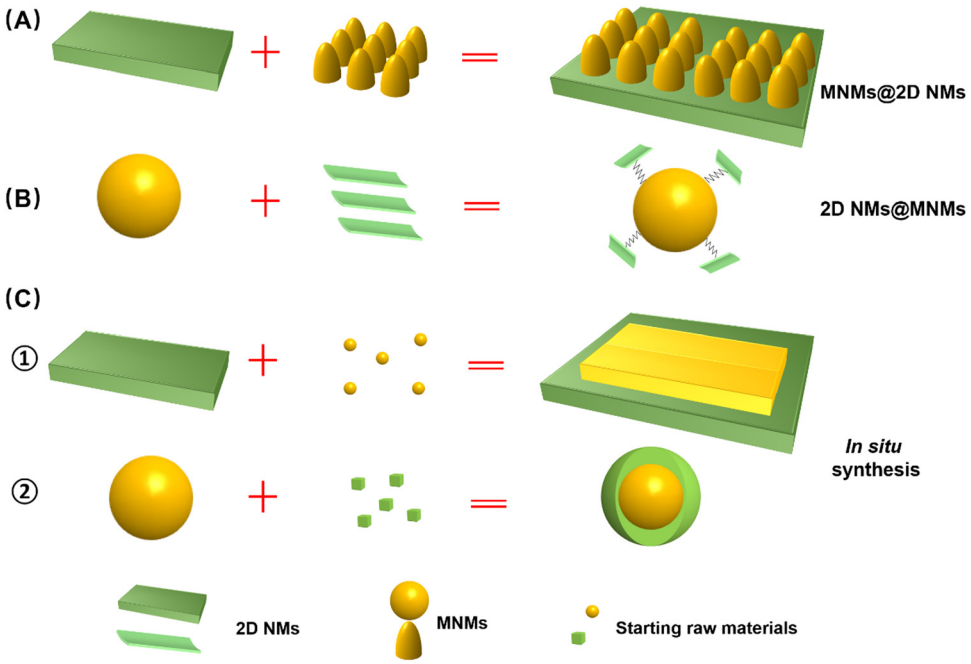


Fig. 3 Schematic illustration of the synthesis strategies for advanced multifunctional M2D NCs. (A) Synthesis of 2D NMs on the MNMs composite (2D NMs@MNMs). (B) Synthesis of 2D NMs on the MNMs composite (2D NMs@MNMs). (C) ① *In situ* synthesis of MNMs on 2D NMs; ② *In situ* synthesis of 2D NMs on MNMs.

magnetic performance compared to alternative structures. Additionally, the small 2D NMs are shielded from rapid degradation by anchoring onto MNMs.

### 3.3 Synthesis of *in situ* growth of one on the other

In addition to the aforementioned composite structure type and synthetic pathways, it is also plausible that *in situ* synthesis of MNMs (Fig. 3C1) or 2D NMs (Fig. 3C2) onto the other one forms a nanohybrid. Liu *et al.* achieved the *in situ* growth of superparamagnetic $Fe_3O_4$ NPs on the surface of $Ta_4C_3$ by redox reaction, followed by coating with soybean phospholipids (SP) to prepare $Ta_4C_3$-IONP-SPs nanocomposites that exhibited superior performance in PTT therapy and NIR imaging.[61] $MnFe_2O_4$-MOFs nanocomposites were synthesized *via in situ* growth of MOFs on the surface of $MnFe_2O_4$ NPs. Initially, $MnFe_2O_4$ NPs were prepared through the thermal decomposition of metal acetyl acetone precursors, and subsequently modified with polyvinylpyrrolidone (PVP). Subsequently, PVP-modified $MnFe_2O_4$ was utilized as the supporting material to selectively adsorb $Zr^{4+}$ ions and tetranuclear (4-carboxyphenyl) porphyrin (TCPP), facilitating the growth of MOFs on its surface and resulting in the formation of a well-defined nanocomposite structure (Fig. 3B).[119] This strategy affords a diverse composite structure for M2D NCs, unconstrained by the intrinsic structure of single MNMs or 2D NMs. Through well-designed chemical reactions, these materials demonstrate a more controllable synthesis, a more stable composition, and a more ordered structure. The myriad structures enhance the versatility of M2D NCs, significantly amplifying their effectiveness and broadening their range of applications.

## 4. M2D NCs and their multimodal antitumor applications

After the meticulous design and construction, advanced M2D NCs not only exhibit enhanced optical/magnetic performance compared to their individual components, but also demonstrate synergistic effects that lead to unexpected biological responses or exotic behaviors in the tumor microenvironment (TME), thus opening up new avenues for antitumor nanotechnologies. In this section, we systematically elucidate different types of M2D NCs used for tumoricidal purposes based on their structure categories of 2D NMs (Table 2), incorporating our innovative ideas in devising fabrication processes and therapeutic/imaging modalities, as well as highlighting their remarkable antitumor advantages.

### 4.1 Magnetic 2D graphene nanocomposites and their multimodal antitumor applications

Due to their inherent distinctive physical and chemical properties, graphene and its derivatives, as the most popular two-dimensional $sp^2$ carbon NMs, have been extensively utilized in biosensing, bioimaging, drug/gene delivery and various types of cancer therapies.[47] Graphene oxide (GO) has been more frequently employed than graphene in constructing nanocomposites due to its better stability in physiological environments. When a magnetic component is elaborately introduced into GO-based materials, the resulting magnetic nanocomposites acquire additional magnetic responsive properties that extend antitumor applications, such as magnetic field-enhanced

 

Table 2 Summary of representative advanced M2D NCs for tumor therapy and imaging based on the components of 2D NMs

| 2D NMs type | M2D NCs | Type of tumor | Therapeutic modalities | Imaging modalities | Stimulus source |
|---|---|---|---|---|---|
| GO | GO-IONP-PEG-DOX[46] | 4T1 tumor | PTT/magnetically targeted drug delivery | MRI | Static magnetic field/808 nm laser |
| | FeMn-GO[47] | MCF-7/ADR/MDA-MB-231 tumor | MHT/chemotherapy | MRI | Alternating magnetic field/pH |
| | RGO-IONP-PEG[39] | 4T1 tumor | PTT | MRI/PAT | 808 nm laser |
| | GQD-MMSNs-DOX[48] | 4T1 tumor | PTT/MHT/chemotherapy | — | Alternating magnetic field/ 808 nm laser |
| | HMNS/$SiO_2$/GQD[49] | Eca-109 tumor | PTT/PDT/magneto-mechanical/ chemotherapy | — | Alternating magnetic field/ 808 nm laser |
| | $MnFe_2O_4$@$SiO_2$@GQDs/DAU[50] | MCF-7/HEK-293 tumor | DAU delivery | — | Static magnetic field/pH |
| | $MnO_2$@Pd@PPy/GO[51] | MCF-7 tumor | PTT/CDT | MRI | 808 nm laser |
| | Cur/GQDs-$Fe_3O_4$-FA[52] | MCF-7/MDA-MB-231 tumor | Cur delivery | — | pH |
| TMDs | $WS_2$-IO@MS-PEG-DOX[53] | 4T1 tumor | PTT/DOX delivery | MRI/CT/PAT | 808 nm laser/pH |
| | $WS_2$:$Gd^{3+}$-PEG[54] | 4T1 tumor | PTT/radiotherapy | PAT/CT/MRI | X-ray RT/808 nm laser |
| | $MoS_2$/$Fe_3O_4$[55] | HeLa and HepG2 tumor | PTT/magnetically Targeted photothermal therapy | MRI/PAT | Static magnetic field/808 nm laser |
| | $MoS_2$-IO-PEG[56] | 4T1 tumor | PTT | PET/PAT/MRI | 808 nm laser |
| | Mo@Fe-ICG/Pt[57] | HeLa tumor | PTT/PDT/ chemotherapy | MRI/IR/PAT | 808 nm laser |
| MXenes | MnOx/$Ti_3C_2$[58] | 4T1 tumor | PTT | MRI/PAI | 808 nm laser/pH |
| | MnOx/$Ta_4C_3$[59] | 4T1 tumor | PTT | MRI/CT/PAI | X-ray/808 nm laser |
| | $Ti_3C_2$-IONP-MXene[60] | 4T1 tumor | PTT | MRI | X-ray/808 nm laser |
| | $Ta_4C_3$-IONP-SPs[61] | 4T1 tumor | PTT | MRI/CT | X-ray/808 nm laser |
| | $Ti_3C_2$–$Fe_3O_4$@$SiO_2$-FA[62] | HeLa tumor | Cisplatin delivery and chemotherapy | — | Static magnetic field/pH |
| | FTC[63] | MKN45 tumor | PTT/CDT | MRI | 808 nm laser |
| BPNSs | BPs@Au@$Fe_3O_4$[64] | U14 tumor | PTT/PDT | MRI | Static magnetic field/650 nm laser/pH |
| | $R^e$-$MnO_2$-$F^f$BP[65] | HeLa tumor | PDT | MRI/FI | 660 nm laser/pH |
| | BPN/$MnO_2$/DOX[38] | HeLa tumor | PDT/PTT/ chemotherapy | MRI/IR | 660 nm laser/808 nm laser |
| | MUCNPs@BPNS-Ce6[66] | HeLa tumor | PTT/PDT | MRI/FI | 808 nm laser |
| | BPNS-Arg-GOx@$MnO_2$ (BAGM)[67] | MCF-7 tumor | PTT/starvation therapy/NO gas therapy | MRI/US | 808 nm laser |
| | RGD-BPNS@SMFN[15] | HeLa tumor | PTT/PDT | — | 660 nm laser/808 nm laser |
| | BPQDs@DOX@ss-$Fe_3O_4$@C-EGFR NPs[68] | HeLa/C6/A549/MCF-7 tumor | Chemotherapy/PTT | MRI/FI | Static magnetic field/808 nm laser/pH |
| LDHs | LDH-Gd/Au[69] | L929 and HeLa tumor | Dox delivery and chemotherapy | CT/MRI | pH |
| | Mn-LDH[70] | B16F10 tumor | dsDNA-cy5 delivery | MRI | pH |
| | MnFe-LDH-MTX[71] | HeLa and HepG2 tumor | MTX delivery and chemotherapy | MRI | pH |
| | Mn-LDH-siRNA[72] | Neuro-2a tumor | siRNA delivery | MRI | pH |
| | $Fe_3O_4$@LDH-MTX[128] | MCF-7 and HepG2 tumor | MTX delivery and chemotherapy | — | pH |
| | LDHs/$Fe_3O_4$@dextran/DOX[73] | — | DOX delivery | — | pH |
| | FA-BSA/$Fe_3O_4$@LDH/5-Fu[74] | HepG2 tumor | 5-Fu delivery | — | pH |
| 2D MOFs | $Fe_3O_4$/ZIF-8-$Au_{25}$[75] | HeLa tumor | Magnetically targeted photodynamic/PTT | MRI | Static magnetic field/808 nm laser |
| | $Mn_3O_4$-PEG@C&A[76] | 4T1 tumor | Nucleus-targeted PDT enhanced by CAT and GSH consumption properties | — | 660 nm laser |
| | Co-Fc@GOx[77] | 4T1 tumor | Cascade enzymatic/Fenton catalytic ROS | — | pH |
| | Fe@ZIF-8@GOx[78] | HeLa tumor | Magnetically triggered enhanced uptake | — | Static magnetic field |
| 2D COFs | $Fe_3O_4$@COF-DhaTph[79] | MCF-7 tumor | PDT/PTT | MR/PAI/IR | 660 nm laser |
| | COF-Au–$MnO_2$-HA[80] | BALB/C tumor | PDT/catalytic cascade reaction | — | 650 nm laser |
| | $Fe_3O_4$@COF-BSA-FA[81] | HeLa tumor | PTT/chemotherapy | — | Static magnetic field/808 nm laser |
| Other 2D NMs | Pd@OH-BNNSs/DOX[82] | MCF-7 tumor | PTT/chemotherapy | — | 808 nm laser/pH |
| | $FePSe_3$@APP@CCM[83] | CT26 tumor | Immune therapy/PTT | MRI/PAI/IR | Static magnetic field/808 nm laser |
| | $C_3N_4$-Fe-TPP NF/MB[84] | HeLa tumor | PDT | MRI | 650 nm laser |

tumor targeting and imaging, or magnetothermally triggered drug release.

As the representative MNMs, IONP was initially employed as a building block for constructing M2D graphene CNs. For instance, the GO-IONP-PEG-DOX complex mentioned above was employed as an MRI-guided PTT/chemotherapy antitumor nanoplatform.[46] Another GO-based MNMs, denoted as a GO-$Fe_3O_4$ nanocomposite, was prepared *via* chemical precipitation method by doping superparamagnetic $Fe_3O_4$ into GO.[93] The resulting MNMs exhibited favorable superparamagnetic properties with a saturation magnetization ($M_s$) of 47.56 emu $g^{-1}$, and could reach 92.8 °C after only 500 s exposure to an alternating current magnetic field (ACMF), demonstrating their enhanced magnetothermal properties that benefit solid tumor eradication. Elham *et al.* devised a magnetically-targeted multifunctional nanocarrier denoted as Cur/GQDs-$Fe_3O_4$-FA. $Fe^{2+}$ and $Fe^{3+}$ were chemically co-precipitated onto GQDs for producing a magnetic nanocomposite, then curcumin (Cur) and conjugating folic acid (FA) were loaded to obtain the cancer-targeting agent (Fig. 4A1).[52] This nanoagent exhibits superparamagnetic behavior ($M_s$ = 60.6 emu $g^{-1}$), and can be guided to the malignancy site by an applied magnetic field and FA without endangering healthy tissues (Fig. 4A2). It was found that 33% of the total curcumin was released after 150 h (Fig. 4A3), then the cell viability of MCF-7 cells treated with Cur/GQDs-$Fe_3O_4$ and Cur/GQDs-$Fe_3O_4$-FA is 31% and 25%, respectively (Fig. 4A4). Similarly, Tao *et al.* fabricated a nano-drug carrier MGO-MDP-FA with 30.18 emu $g^{-1}$ by covering the surface of $Fe_3O_4$-modified graphene oxide (MGO) with folic acid-grafted maltodextrin polymers (MDP-FA) (Fig. 4B1 and B2).[120] DOX showed a maximum loading capacity of 657.9 mg $g^{-1}$ and 39.68 wt% *via* π–π, hydrogen bond and hydrophobic interactions (Fig. 4B3). This nanoagnet showed excellent chemo-photothermal synergistic tumor inhibition *in vitro* (tumor cell killing rate reached 80%) (Fig. 4B4).

In addition to IONP, other MNMs are sequentially incorporated into the graphene- based nanocomposite. Chen *et al.* fabricated a FeMn-GO composite using a dual redox strategy that involved the *in situ* synthesis of superparamagnetic $Fe_3O_4$ and paramagnetic $MnO_x$ onto exfoliated GO nanosheets.[47] By virtue of its exceptional magnetic properties, high drug loading capacity, and disintegration behavior in a mildly acidic environment, the resulting FeMn-GO exhibits remarkable stimulus-responsive therapeutic and imaging capabilities. These include pH-responsive MRI and drug release, redox-responsive MRI, as well as magnetic-responsive MRI-guided hyperthermia. More importantly, this platform effectively inhibits tumor metastasis and dramatically reverses the multidrug resistance. Zahra *et al.* developed a pH-sensitive nanoplatform utilizing a fluorescence resonance energy transfer (FRET) system, $MnFe_2O_4$@$SiO_2$@graphene quantum dots with a saturation magnetization of 28.02 emu $g^{-1}$ (Fig. 4C1–C3). MTT assay results indicate that the nanoplatform induces cell apoptosis by inhibiting the growth of more than 95% of the MCF-7 cells (Fig. 4C4).[50]

### 4.2 Magnetic 2D transition metal dichalcogenides (TMDs) nanocomposites and their multimodal antitumor applications

2D TMDs are a prominent class of graphene analogues that have garnered significant interest due to their diverse composition, consisting of monolayers of $MX_2$ where M is a transition metal and X is a chalcogen element such as S, Se, or Te.[101] TMDs can exist in the form of either triangular or octahedral prisms. Examples of representative TMDs include $MoS_2$, $WS_2$ and $MoSe_2$, which can be prepared by various methods such as mechanical exfoliation, lithium-ion intercalation, liquid exfoliation, and meteorological precipitation.[96] The utilization of $MoS_2$ nanosheets as an effective PTT agent for tumor ablation was firstly reported by Chou *et al.*[49] Since then, numerous TMDs-based MNMs have also been fabricated for diverse antitumor applications.

TMD nanosheets exhibit an ultrahigh specific surface area and a large number of active sites, facilitating efficient binding with MNMs. For instance, Yang *et al.* designed a multifunctional nanoplatform $WS_2$-IO@MS-PEG-DOX by encapsulating abundant IONP and DOX. In addition to possessing a series of inherent fine physical properties, the nanoplatform presents NIR laser-triggered drug release behavior, enabling CT imaging-guided dual PTT/chemotherapy upon laser irradiation (Fig. 5A1–A3).[53] The nanoplatform realized effective tumor ablation, delivered excellent *in vivo* synergistic therapeutic effect of photothermal and chemotherapy under laser stimuli (Fig. 5A4). Additionally, the ultrahigh photoconversion efficiency is highly suitable for the implementation of PDT. Moreover, when doped with MNMs, multimodal tumor bioimaging can be readily achieved through CT, MRI, fluorescence imaging (FI) and photoacoustic imaging (PAI) techniques. Cheng *et al.* developed $Gd^{3+}$-doped $WS_2$ nanosheets modified with PEG ($WS_2$:$Gd^{3+}$-PEG) for enhanced radiotherapy/PTT guided by PA/CT/MR imaging. $WS_2$ exhibited strong NIR absorption and X-ray attenuation, enabling it to serve as a contrast for PAI and CT. Additionally, the introduction of $Gd^{3+}$ doping enhanced its MRI properties.[54] Collectively, the trimodal imaging approach demonstrated that $WS_2$:$Gd^{3+}$-PEG rapidly accumulates in tumor tissues following intravenous injection (Fig. 5B1 and B2). The nanocomposite realized the inhibition of tumor growth completely under NIR and X-ray irradiation, demonstrating the remarkable advantage of combination therapy in comparison to monotherapy (Fig. 5B3). Yu *et al.* prepared biocompatible PEG-$MoS_2$/$Fe_3O_4$ composites (MSIOs) by a simple two-step hydrothermal method, which served as a bimodal $T_2$-MRI and PAI agent for precise real-time monitoring of PTT.[55] Similarly, Liu *et al.* synthesized $Fe_3O_4$ NPs with a homogeneous nanoflower shape in sizes ranging from 80–180 nm by hydrothermal method, and then covalently grafted onto polyimide (PEI)-functionalized $MoS_2$, finally encapsulating into indocyanine green (ICG) molecules and Pt(IV) precursors, resulting in $MoS_2$@Fe-ICG/Pt nanocomposites (Fig. 5C1).[57] The incorporation of ICG into the composites conferred additional NIR imaging properties, enabling remarkable trimodal NIR/MR/PA imaging-guided PTT, PDT, and chemotherapeutic synergistic treatment triggered by a single 808 nm NIR laser (Fig. 5C2).

 

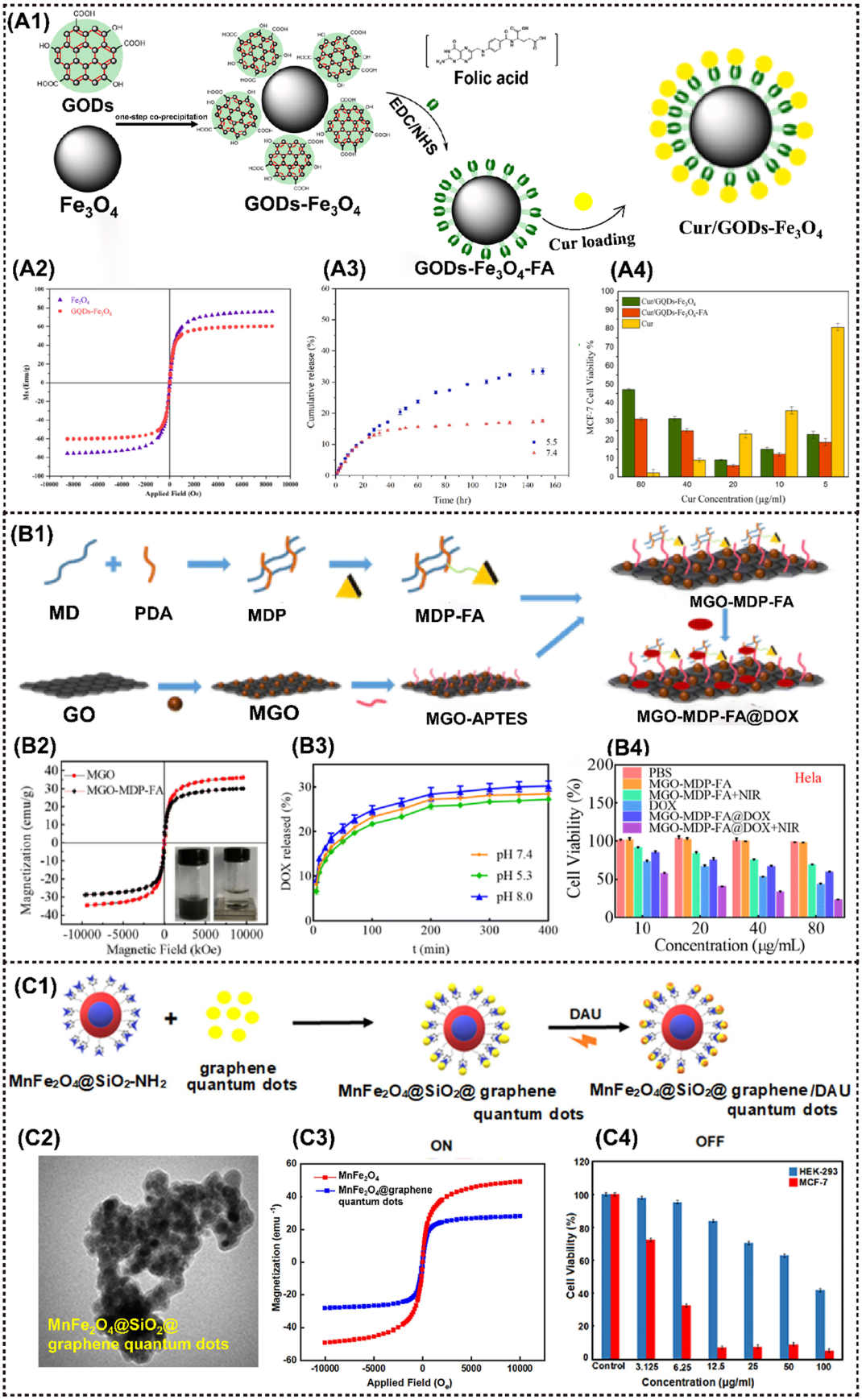


Fig. 4 Advanced magnetic 2D graphene nanocomposites for cancer therapy and drug delivery. (A1) Schematic diagram of the Cur/GQDs-$Fe_3O_4$-FA preparation. (A2) Magnetic hysteresis loop of $Fe_3O_4$ and GQDs-$Fe_3O_4$. (A3) Cumulative release of curcumin at pH values of 5.5 and 7.4 from Cur/GQDs-$Fe_3O_4$-FA. (A4) Cell

viability profiles of Cur, Cur/GQDs-$Fe_3O_4$, and Cur/GQDs-$Fe_3O_4$-FA after 48 h incubation. Reproduced with permission.[52] Copyright 2023, Elsevier. (B1) The synthetic route of the MGO-MDP-FA nano-drug carrier. (B2) Magnetic hysteresis loop of MGO and MGO-MDP-FA. (B3) The drug releasing rate of DOX from MGO-MDP-FA in PBS with pH 7.4 and 5.3 at 37 °C. (B4) Cell viability of HeLa treated with PBS, MGO-MDP-FA, MGO-MDP-FA + NIR, DOX, MGO-MDP-FA@DOX and MGO-MDP-FA@DOX + NIR. Reproduced with permission.[120] Copyright 2023, RSC Advances. (C1) Schematic diagram of DAU loading on $MnFe_2O_4$@$SiO_2$@GQDs. (C2) TEM image of $MnFe_2O_4$@$SiO_2$@GQDs. (C3) Magnetic hysteresis loop of $MnFe_2O_4$@$SiO_2$@GQDs. (C4) Cell viability for the HEK-293 normal cells and MCF-7 cancer cells in various concentrations of $MnFe_2O_4$@$SiO_2$@GQDs/DAU after 48 h incubation. Reproduced with permission.[50] Copyright 2022, Elsevier.

*In vitro* and *in vivo* results showed that the as-fabricated Mo@Fe-ICG/Pt nanocomposites exhibit good MR/IR/PA trimodal imaging capacity and conspicuous PDT/PTT/chemo-combined effect (Fig. 5C3 and C4).

### 4.3 Magnetic 2D transition metal carbide/nitride/carbonitride (MXenes) nanocomposites and their multimodal antitumor applications

A significant type of multifunctional 2D NMs, known as MXenes, comprises various transition metal carbides and carbonitrides. MXenes demonstrate enhanced hydrophilicity for *in vivo* application compared to 2D graphene and TMD NMs due to the presence of fluorine, oxygen, or hydroxyl groups and stronger NIR absorption. 2D MXenes such as $Ti_3C_2$ and $Ta_4C_3$ were first prepared by exfoliating MAX compounds with the general formula $M_{n+1}AX_n$, where *M* represents a transition metal, A denotes a group 13 or 14 element, X stands for carbon or nitrogen, and n ranges from 1 to 3. The formula for MXenes is represented by $M_{n+1}X_nT_x$, where T denotes the surface termination group (=O, –F, or –OH), and *x* indicates the number of surface functional groups.[121] Chen *et al.* reported the utilization of $Ti_3C_2$ nanosheets with a remarkable photothermal conversion efficiency (PTCE) of 30.6% for efficient tumor thermotherapy and recurrence prevention under laser irradiation, highlighting the immense application potential of MXenes-based nanomaterials *in vivo*.[122]

MXenes are a suitable nanocarrier due to their typical 2D planar topology, which facilitates the loading of MNMs onto the laminar surface.[123] Chen *et al.* successfully constructed $MnO_x$/$Ti_3C_2$ nanocomplexes by *in situ* growth of small $MnO_x$ nanosheets on the surface of $Ti_3C_2$ MXenes based on their specific surface activity through a facile redox reaction. These nanocomplexes were developed as a multifunctional theranostic platform for MRI/PAI dual-modal imaging-guided PTT. It is noteworthy that the modification of the $MnO_x$ component has enabled the nanocomplex to show $T_1$-MRI performance that is responsive to stimuli of TME, resulting in significant inhibition of tumor growth.[58,124]

A similar strategy was reported in $MnO_x$/$Ta_4C_3$ nanocomposites for MRI/CT/PAI guided PTT against cancer. The incorporation of Ta, with its high atomic number, into $MnO_x$/$Ta_4C_3$ rendered excellent contrast enhancement for CT imaging. In addition, the integrated $MnO_x$ component demonstrated TME-responsive $T_1$-MRI behavior, while the inherent PAI performance originated from MXenes. Moreover, the nanocomposites achieved a remarkable PTCE of up to 34.9%, leading to complete tumor eradication in mice (Fig. 6A1–A3).[59] Liu *et al.* synthesized a $Ti_3C_2$-IONP-MXenes nanohybrid by *in situ* growth of small superparamagnetic $Fe_3O_4$ nanocrystals on the surface of $Ti_3C_2$ MXenes, which present high $T_2$-MR relaxation rates (394.2 $mM^{-1}$ $s^{-1}$), thus showing great potential for MRI-guided therapy.[65] Subsequently, $Ta_4C_3$-IONP-MXenes were fabricated using a similar method, resulting in enhanced CT and MRI performance due to the high X-ray attenuation coefficient and the ordered integration of superparamagnetic IONP. This successively enabled the dual-modal imaging-guided PTT for breast tumor.[61] Furthermore, Wu *et al.* anchored $Fe^{2+}$ ions into the layers of 2D ultrathin TC nanosheets (TC NSs) to synthesize a multifunctional nanoshell of Fe(II)–$Ti_3C_2$ (FTC) through interlayer electrostatic adsorption (Fig. 6B1).[63] The coupling of Fe (II) ions enhanced the tumoricidal activity by photothermal and chemodynamic therapy (Fig. 6B2), and achieved MRI (Fig. 6B3). The development of titanium carbide magnetic core–shell nanocarriers ($Ti_3C_2$–$Fe_3O_4$@$SiO_2$-FA) by Mahdieh *et al.* is particularly noteworthy given that it allows for pH-responsive drug release (Fig. 6C1) and magnetic manipulation (Fig. 6C2).[62] The findings demonstrated that the utilization of magnetism to regulate cisplatin release resulted in enhanced suppression of tumor growth by $Ti_3C_2$-$Fe_3O_4$@$SiO_2$-FA nanocarriers (Fig. 6C3).

### 4.4 Magnetic 2D black phosphorus (BPs) nanocomposites and their multimodal antitumor applications

Phosphorene, also known as black phosphorus nanosheets (BPNSs), demonstrated an exceptionally high surface area and volume ratio owing to their puckered honeycomb structure composed of phosphorus atoms. It has been reported that the loading capacity of DOX on the BPNSs' surface can reach up to 950% in weight, surpassing that of other 2D materials systems.[125] Therefore, the abundance of active sites on the BPNS surface is advantageous for anchoring MNMs, resulting in the magneto-responsive nanocomposites.

Zhang *et al.* developed a novel theranostics platform based on BPNS, which integrates small $Fe_3O_4$@$MnO_2$-doped $NaYF_4$:Yb/Er/Nd UCNPs (MUCNPs) and chlorin e6 (Ce6) on the ultrathin BPNS to fabricate MUCNPs@BPNS-Ce6. This platform can be used for optical imaging and PDT *in vivo* (Fig. 7A1). The nanoplatform exhibits a high photosensitizing efficiency and saturation magnetization (Fig. 7A2). Initially, PTT was activated by 808 nm laser irradiation, followed by adjustment to 660–670 nm, enabling flexible operation of PDT in both BPNS and Ce6. During the hyperthermia process, $Mn^{2+}$ decomposed from $MnO_2$ and catalyzed excessive intracellular $H_2O_2$ in acidic TME to efficiently generate $O_2$ through the Fenton reaction, which was crucial for enhancing PDT. Additionally, the obtained $Mn^{2+}$ provided explicit $T_1$-MRI signal, while $Fe_3O_4$ served as the $T_2$-MRI contrast agent and Ce6 acted as a FI probe, collectively



 

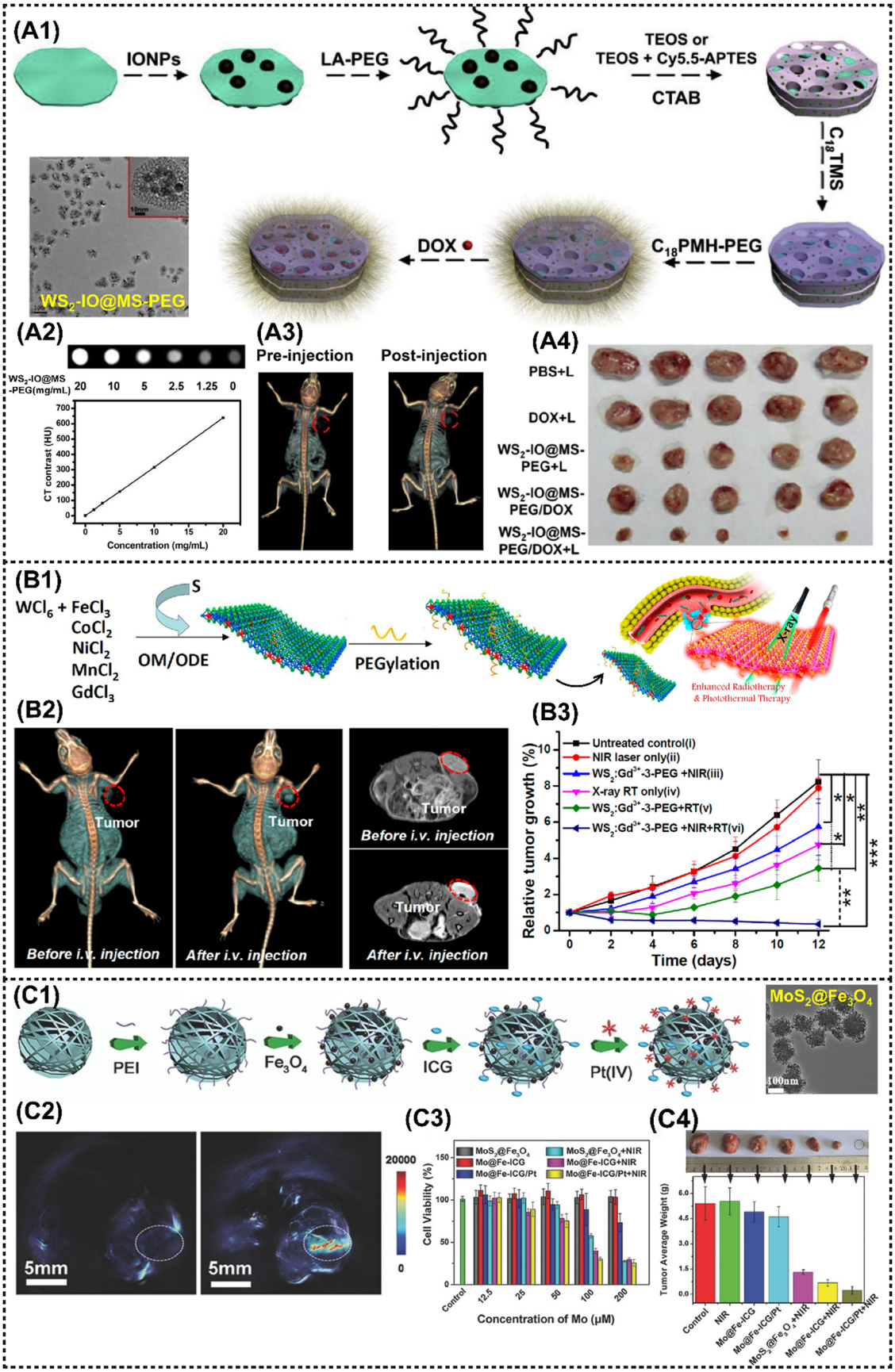


Fig. 5 Advanced 2D TMDs nanocomposites for cancer therapy and imaging. (A1)–(A3) A procedure showing the fabrication of $WS_2$-IO@MS-PEG/DOX and the application in CT imaging-guided tumor treatment. (A4) The photographs of 4T1 tumors excised from mice at the end of treatments (day 14).

Reproduced with permission.[53] Copyright 2015, Elsevier. (B1) Scheme to show the one-pot synthesis of metal-ion-doped $WS_2$ nanoflakes and the enhanced radiotherapy/PTT route. (B2) *In vivo* CT images (left) and $T_1$-weighted MR images (right) of mice before and 24 h after i.v. injection with $WS_2$:$Gd^{3+}$-PEG. (B3) Tumor volume growth curves of mice after various treatments. Reproduced with permission.[53] Copyright 2015, ACS. (C1) A scheme showing the preparation process of Mo@Fe-ICG/Pt nanocomposites. (C2) The *in vivo* PA images of the tumor-bearing mice before (left) and after (right) the injection of Mo@Fe-ICG. (C3) *In vitro* cytotoxicity of different stimulations against HeLa cells after 24 h incubation. (C4) The photographs and the mean tumor weights of the excised tumors after various treatments. Reproduced with permission.[57] Copyright 2017, Wiley-ACH.



resulting in the impressive multimodal imaging performance *in vivo* (Fig. 7A3).[66] Photographs of excised tumors verified the safety and enhanced antitumor effect of this nanoplatform (Fig. 7A4).

Liu *et al.* developed a magnetic nanoplatform based on BPNS termed as $R^e$-$MnO_2$-$F^f$BP. This platform was modified with fluorescein isothiocyanate (FITC)-labelled peptide-functionalized BPNS, and incorporated with rhodamine B (RhB) encapsulated-manganese dioxide ($R^e$-$MnO_2$). It enables bimodal monitoring of oxygen self-supply and enhanced PTT.[65] The multifunctional $R^e$-$MnO_2$-$F^f$BP nanoplatform demonstrated striking synergistic effect in delivering continuous local $O_2$ to overcome hypoxia and boost the PDT performance. Simultaneously, the released $Mn^{2+}$ and RhB dye were employed for dual-mode MRI/FI, enabling real-time monitoring of the oxygen self-supply process as a feedback mechanism for therapeutic efficacy. Yang *et al.* prepared a BPs@Au@$Fe_3O_4$ nanohybrid for MRI-monitoring PTT and PDT on HeLa tumors in mice. Compared to the three individual materials of BPNSs, BPs@Au and BPs@$Fe_3O_4$, the BPs@Au@$Fe_3O_4$ nanohybrid demonstrated superior tumor inhibition efficacy *in vivo* when triggered by a 650 nm laser radiation and an external magnetic field. The synergistic antitumor performance can be attributed to the well-ordered hybrid nanostructure, rather than a simple summation of the individual functional components.[64]

The potential of the BPNS-based MNMs has also been investigated as an intelligent nanozyme or nanoreactor system. Our group proposed a biocompatible and targeted delivery PTT–PDT self-synergetic nanoplatform, denoted as RGD-BPNS@SMFN, based on temperature-dependent catalase (CAT)-like behavior for efficient tumor elimination. It was found that the PTT-promoted inherent CAT-like activity within the nanoplatform remodels the tumor hypoxic microenvironment, thereby ameliorating the PDT efficiency and providing a synergetic dual-mode PTT/PDT approach with exceptional performance (Fig. 7B1).[15] It was determined that BPNS@SMFN has the highest saturation magnetization (150.0 emu $g^{-1}$) (Fig. 7B2). *In vitro* and *in vivo* experiments further indicated the optimal tumor synergetic treatment outcomes compared to the monotherapy of BPNS or SMFN (Fig. 7B3 and B4). Su *et al.* innovatively constructed a novel nanozyme system termed BPNSs-Arg-GOx@$MnO_2$ (BAGM), which served as a multimodal synergistic therapeutic platform. The BAGM nanozyme effectively initiates a cascade reaction by depleting intracellular glucose to generate $H_2O_2$, subsequently converting $H_2O_2$ into $O_2$ within the acidic microenvironment of cells and thereby facilitating the oxidation of L-Arg to nitric oxide (NO). Thereafter, NO production can activate matrix metalloproteinases to degrade the dense extracellular matrix (ECM) in solid tumors and convert collagen within the matrix into a more porous state. In turn, this heightened the accumulation of the BAGM nanozyme within the loose ECM and improves the PTT performance.[67] Similarly, Wu *et al.* engineered a modified BPNS by incorporating $MnO_2$ NPs, resulting in the development of an intelligent self-driven theranostic platform with specific tumor targeting capabilities (Fig. 7C1). The BPNS/$MnO_2$ platform displayed simultaneous pH and redox-responsive MRI performance, as well as drug release behavior. In comparison to bare BPNS, the newly developed BPN/$MnO_2$ nanohybrid achieves 37% increase in PTCE and an additional 3.8-fold enhancement in PDT within hypoxic TME. The multiple properties responsive to TME provide intelligent MR and thermal imaging, facilitating precise monitoring of drug delivery to the tumor with nearly 4-fold greater release than that that stimulated by acid alone, thereby further reducing potential chemotherapy side effects on normal tissues (Fig. 7C2).[38]

In addition to BPNS, black phosphorus quantum dots (BPQD) have been employed in the construction of M2D NCs. Zhang *et al.* fabricated a multifunctional nanocomposite BPQDs@DOX@ss-$Fe_3O_4$@C-EGFR that is responsive to pH/NIR/glutathione (GSH). Initially, DOX was encapsulated into ss-$Fe_3O_4$@C, then conjugated with PEGylation BPQDs. Finally, the nanocomposite was modified with epidermal growth factor receptor (EGFR) on the outer shell. Specifically, the nanocomposite exhibits significant accumulation within the tumor due to its EGFR active targeting and magnetic orientation, which can be effectively monitored through dual MRI/FI. Furthermore, BPQDs@DOX@ss-$Fe_3O_4$@C showcased significant tumor suppression *in vivo* due to its pH, NIR, and redox-responsive drug release behavior, surpassing the efficacy of mono-phototherapy or chemotherapy, while maintaining high safety on healthy tissues.[68]

### 4.5 Magnetic 2D layered double hydroxides (LDHs) nanocomposites and their multimodal antitumor applications

The layer double hydroxides (LDHs), also referred to as hydrotalcite-like compounds, exhibit the general formula of $[M^{2+}_{1-x}M^{3+}_{x}(OH)_2]^{x+}(A^{m-})_{x/m}\cdot nH_2O$, where M represents metal elements with either divalent or trivalent oxidation states, and A represents interlayer anions.[96] Notably, the majority of LDHs consist of silicate clay-like minerals exhibiting minimal toxicity and high solubility in physiological environment. Consequently, M2D LDHs CNs have been effectively employed in the field of antitumor research through further targeted modifications specific to tumor cells and encapsulation of functional payloads.

Zhao *et al.* developed magnetic $Fe_3O_4$@MTX-LDH/Au NPs encapsulating the anticancer agent of methotrexate (MTX) *via* a

 

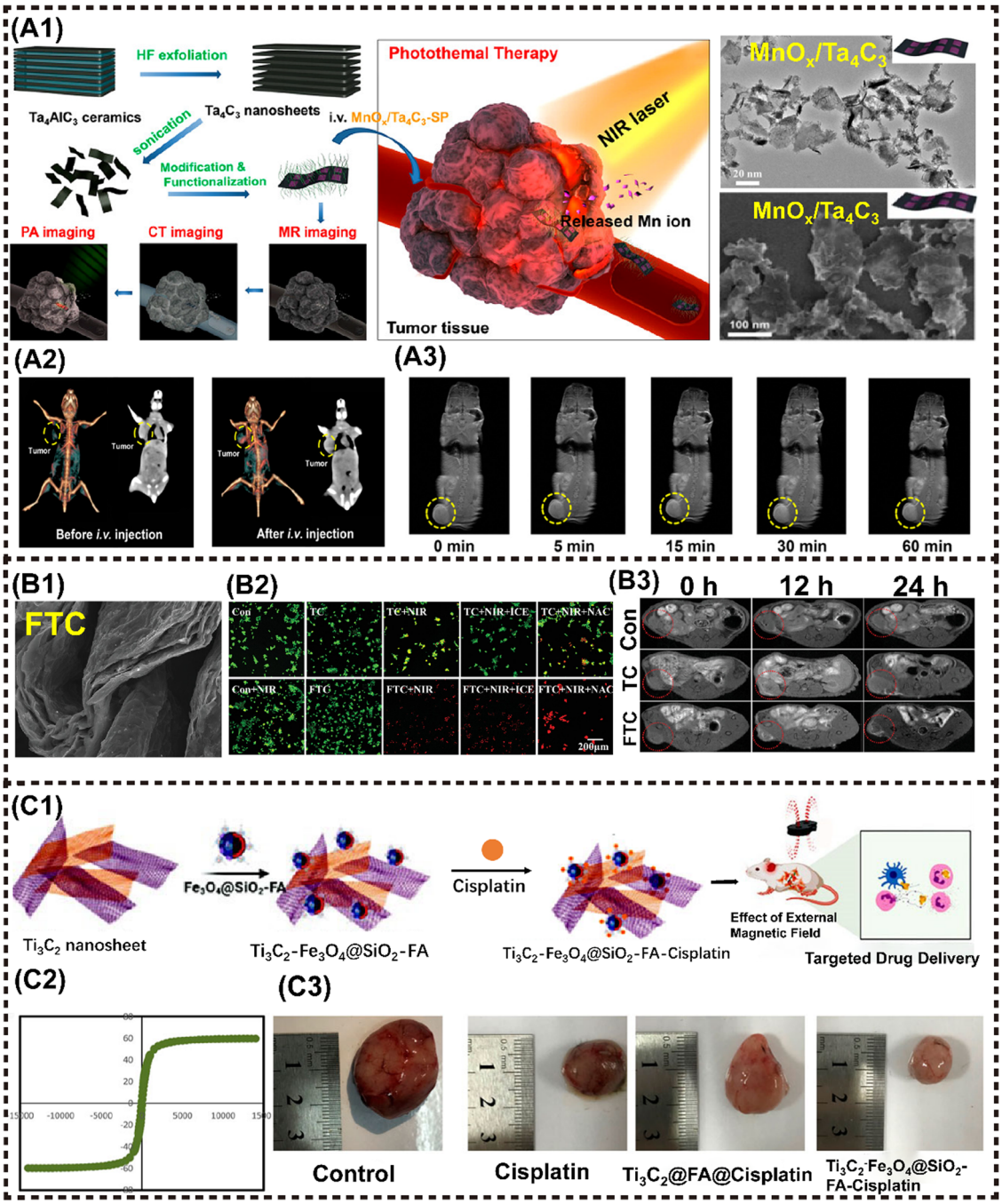


Fig. 6 Advanced magnetic 2D MXenes nanocomposites for cancer therapy and imaging. (A1) Scheme to present the tumor theranostics of the $MnO_x$/$Ta_4C_3$-SP composite for MR/CT/PA imaging-guided PTT. (A2) *In vivo* 3D reconstruction CT (left) and contrast (right) images of mice before and after i.v. administration of the MnOx/$Ta_4C_3$-SP composite nanosheets for 2 h. (B3) $T_1$-weighted imaging of 4T1 tumor-bearing mice after i.v. administration of the MnOx/$Ta_4C_3$-SP composite nanosheets for prolonged time intervals. Reproduced with permission.[59] Copyright 2017, ACS. (B1) FE-SEM pattern of FTC. (B2) Confocal fluorescence images of live (green) and dead (red) cells after different treatments. (B3) MRI images of MKN45 tumor-bearing Balb/c nude mice at different time points after intratumoral injection. Reproduced with permission.[63] Copyright 2021, Wiley-ACH. (C1) Schematic illustration of the fabrication of $Ti_3C_2$-$Fe_3O_4$@$SiO_2$-FA nanoplatforms and cisplatin targeting for cervical cancer delivery *in vivo* study. (C2) Magnetic hysteresis loop of $Ti_3C_2$-$Fe_3O_4$@$SiO_2$-FA. (C3) $Ti_3C_2$-$Fe_3O_4$@$SiO_2$-FA-cisplatin reduces the tumor size in cervical cancer tumors. Reproduced with permission.[62] Copyright 2023, Wiley-ACH.

coprecipitation-electrostatic interaction strategy.[126] Firstly, MgAl-LDH materials were deposited over the surface of $Fe_3O_4$ NPs by the coprecipitation method. Secondly, Au NPs were successfully anchored onto the surface of LDH through electrostatic interaction (Fig. 8A1). These particles presented a well-defined core–shell structure, strong magnetization (Fig. 8A2), and a high drug-loading capacity. Cell lethal test of $Fe_3O_4$@MTX-LDH/Au NPs revealed that the platform exhibited

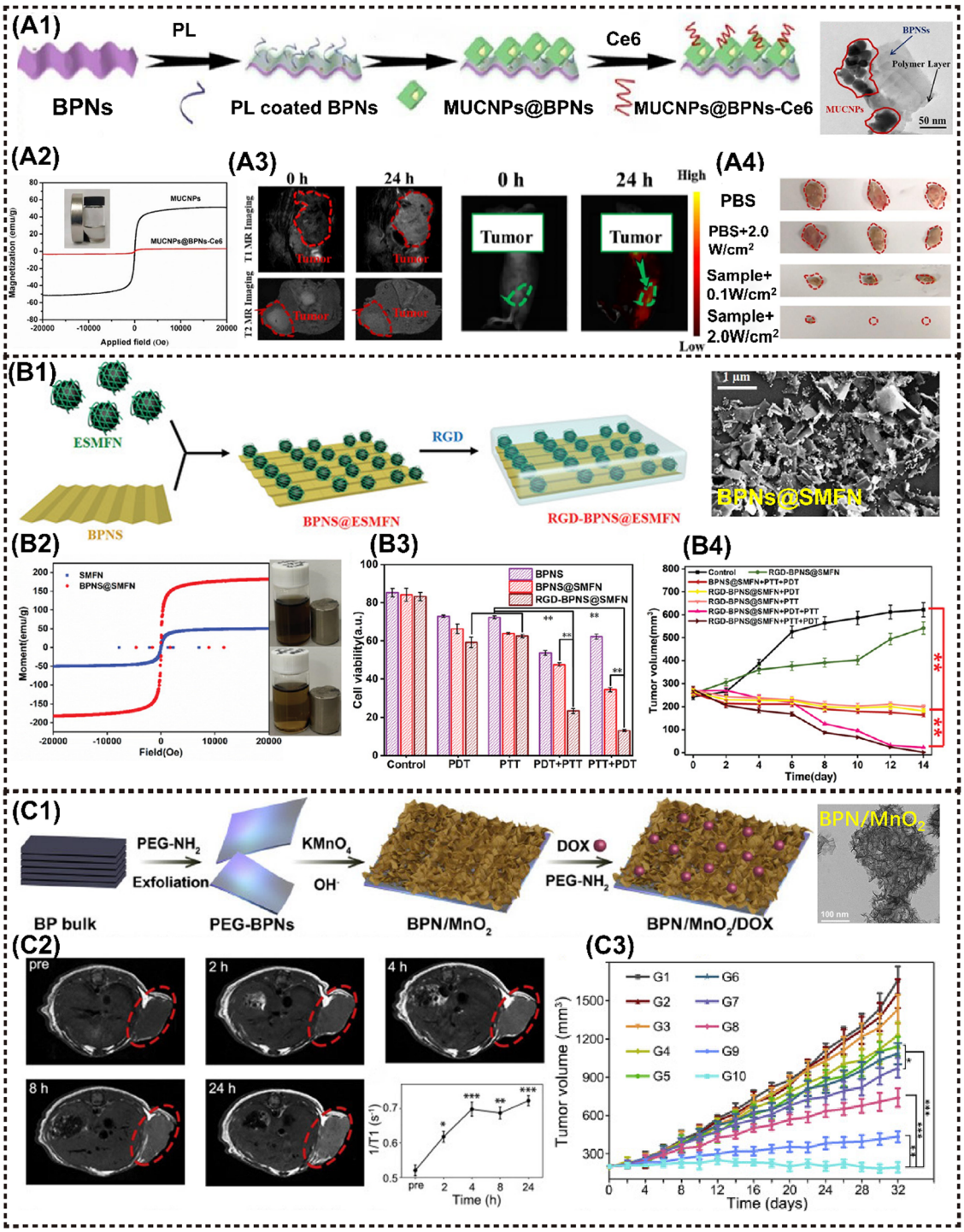


Fig. 7 Advanced magnetic 2D BP nanocomposites for cancer therapy and imaging. (A1) Schematic illustration for the fabrication of MUCNPs@BPNS-Ce6 nanoplatforms. (A2) Magnetic hysteresis loop for MUCNPs and MUCNPs@BPNs-Ce6. (A3) *In vivo* MR images (left) and *in vivo* fluorescence images (right) of the tumor-bearing mice before and after injection with MUCNPs@BPNs-Ce6 for 24 h. (A4) Photographs of excised tumors from mice under different treatment. Reproduced with permission.[66] Copyright 2020, Elsevier. (B1) Schematic illustration for the construction of the RGD-BPNS@SMFN nanoplatform. (B2) The field-dependent magnetic hysteresis loops of the samples. (B3) *In vitro* cell viabilities of HeLa cells after different treatments with nanomaterials as-synthesized. (B4) Tumor volume variation in different treatment groups with time. Reproduced with permission.[15] Copyright 2022, Wiley-ACH. (C1) Schematic presentation of the preparation of multifunctional BPN/$MnO_2$/DOX nanostructures. (C2) *In vivo* MRI of mice bearing HeLa tumors after the intravenous injection of BPN/$MnO_2$/DOX and time-dependent $T_1$ value changes. (C3) Time-dependent tumor growth of mice with different treatments. Reproduced with permission.[38] Copyright 2019, Elsevier.

 

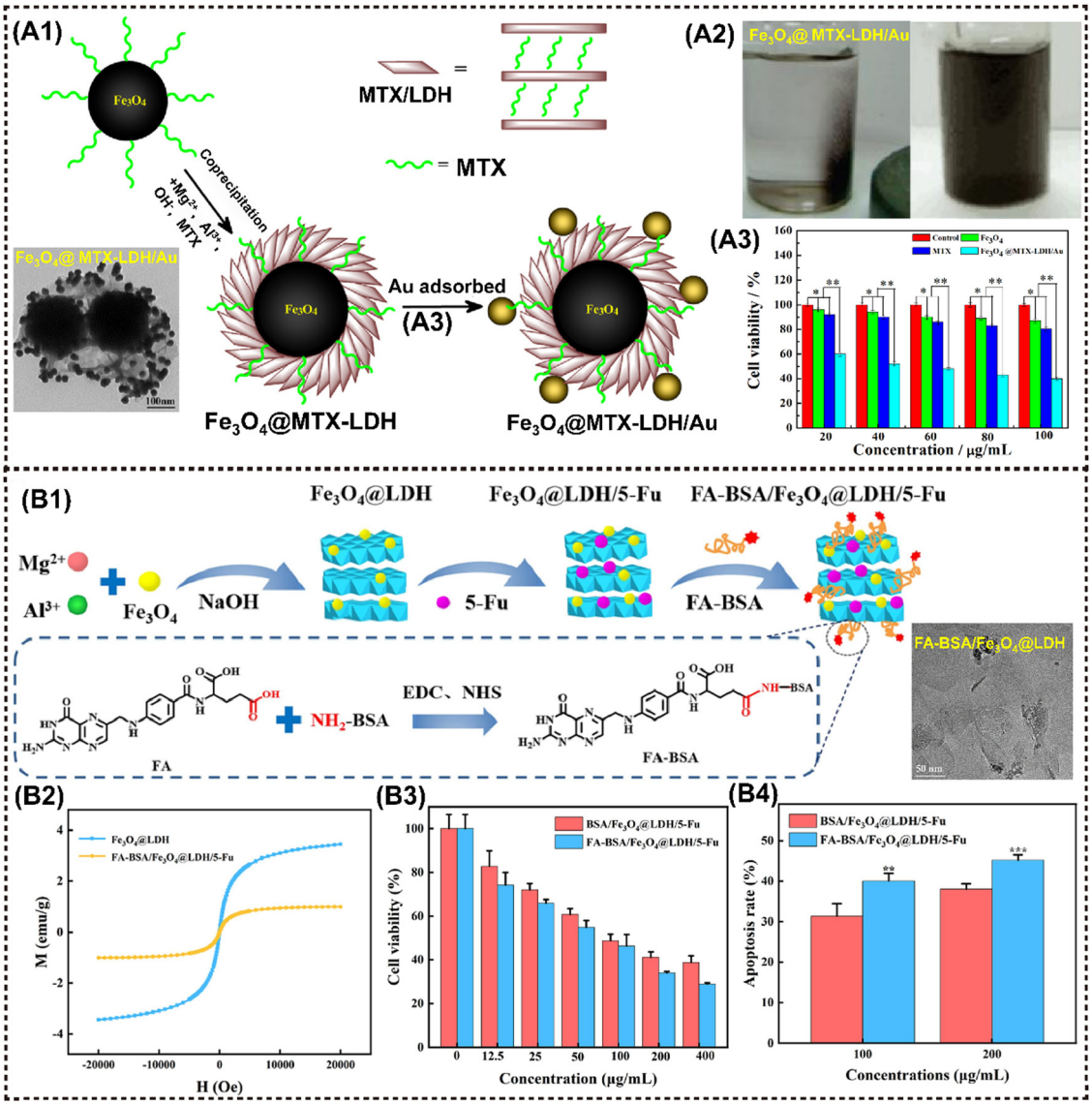


Fig. 8 Advanced magnetic 2D LDHs nanocomposites for cancer therapy and imaging. (A1) Schematic procedure for the preparation of $Fe_3O_4$@MTX-LDH/Au NPs. (A2) Photographs of the $Fe_3O_4$@MTX-LDH/Au NPs in the presence of the external magnet (left), and photographs of the $Fe_3O_4$@MTX-LDH/Au NPs after ultrasonication when removing the external magnet (right). (A3) Comparison of cell viabilities for MTX, $Fe_3O_4$ NPs, $Fe_3O_4$@MTX-LDH/Au NPs at various concentrations after 48 h of incubation. Reproduced with permission.[126] Copyright 2018, Elsevier. (B1) Schematic illustration of the preparation process of FA-BSA/$Fe_3O_4$@LDH/5-Fu. (B2) Magnetic hysteresis loop of different samples. (B3) Cell viability of HepG2 cells after treatment. (B4) Quantitative analysis results of the apoptosis rate of hepatoma cell microspheres. Reproduced with permission.[74] Copyright 2023, Elsevier.

the lowest cell vitality of only 40% (Fig. 8A3). Interestingly, MnAl-LDH serves as a dual-functional platform for MRI and siRNA delivery *via* cellular metabolism pathway, showing improved biosafety and therapeutic efficacy with $r_1$ value of 4.47 $mM^{-1}$ $s^{-1}$ that is even higher than that of commercial contrast agent gadolinium complexes ($r_1$ = 3.4 $mM^{-1}$ $s^{-1}$).[72] Particularly, the cell-death siRNA (CD-siRNA) delivered by Mn-LDH demonstrated stronger lethal effects on brain cancer cells compared to free CD-siRNA.

Introducing magnetic elements or other inorganic NMs into LDH layers through rich intercalation chemistry provides a facile approach to constructing a magnetic nanohybrid. For instance, $Gd^{3+}$ and $Mn^{2+}$ are paramagnetic metal ions that can be utilized in MRI.[127] The LDH-Gd/Au nanocomposite was synthesized by incorporating Gd and Au into LDH, which has been recognized as a multifunctional platform for CT/MR bimodal imaging and simultaneous drug delivery. Interestingly, LDH-Gd/Au displayed an improved dose-dependent positive CT contrast enhancement, with significantly stronger brightness compared to commercial Iobitridol. Moreover, a series of metal-doped LDH nanohybrids have been developed for pH-responsive tumor theranostic platforms, inspired by the disintegrating behavior of metals (Fe, Mn, Gd, *etc.*) and hydroxides in acidic TME. Li *et al.* designed pH-sensitive manganese-based double hydroxide (Mn-LDH) nanocomposites, which demonstrated tumor-specific MRI enhancement rather than

normal tissues in mice.[70] Huang *et al.* reported on manganese-iron layered hydroxides (MnFe-LDH), showcasing excellent responsiveness to acidic TME and releasing paramagnetic $Mn^{2+}$ and $Fe^{3+}$ ions for $T_1$-MRI in tumor regions, as well as delivering chemotherapeutic drugs in a pH-controlled manner.[71] Analogously, Wu *et al.* successfully prepared the nanocomposite $Fe_3O_4$@LDH-MTX by utilizing LDH as a host for both $Fe_3O_4$ and the anticancer drug methotrexate (MTX). The resulting material exhibited significant anticancer activity due to its magnetically guided and pH-responsive drug release properties.[128] Similarly, Liu *et al.* proposed a novel FA-BSA/$Fe_3O_4$@LDH composed of a folic acid-bovine serum albumin conjugate (FA-BSA) conjugated with nano $Fe_3O_4$ and LDH for the delivery of the anticancer drug 5-Fluorouracil (5-Fu) (Fig. 8B1).[74] FA-BSA/$Fe_3O_4$@LDH/5-Fu showed pH-responsive release behavior; the releasing rate is significantly higher in pH 5.0 release medium than that in pH 7.4 release medium (Fig. 8B2). *In vitro* results showed that the nanocomposite resulted in the strongest apoptosis outcomes of hepatocellular carcinoma cells (Fig. 8B3 and B4).

### 4.6 Magnetic 2D MOFs nanocomposites and their multimodal antitumor applications

2D Metal–organic frameworks (MOFs) materials are built by the coordination of metal cations and organic ligands, facilitating their application in various biomedical fields such as biosensing, bioimaging, and disease treatment due to their remarkable functional groups, porous structure, and tunable properties.[96,101] Meanwhile, the efficient biodegradation and rapid renal clearance behavior ensure excellent biosafety within the body. Regarding antitumor applications, MOFs-based NMs generally exhibit superior PDT/PTT/drug delivery behavior and imaging performance, resulting in effective tumor suppression. For instance, Yang *et al.* synthesized $Fe_3O_4$/ZIF-8-$Au_{25}$ nanocomposites as a cooperative therapeutic system by grafting $Au_{25}(SR)_{18}^-$ clusters and $Fe_3O_4$ NPs onto MOFs. This multifunctional magnetic core–shell composites exhibited magnetic targeted trimodal PDT/PTT/MHT capabilities that could be monitored using MRI. *In vivo* experiments further confirmed the synergistic inhibitory effect of combined theranostics on tumor, with fewer side effects on normal organs compared to single PDT or PTT treatment.[75]

The application of cascade nanozyme catalysis therapy in M2D MOFs CNs has been extensively investigated. Zeng *et al.* developed a novel cascade nanozyme $Mn_3O_4$-PEG@C&A using the template of MOFs. The M2D NCs derived from MOFs with intrinsic catalase-like activity engendered the conversion of $H_2O_2$ into $O_2$, thereby enhancing PDT efficacy through simultaneous GSH consumption. The $Mn_3O_4$ NPs were synthesized using MOFs as a substrate, resulting in a larger pore size and surface area compared to native MOFs. The larger pore size and surface area favor the loading of high dose photosensitizer molecules. Following the decoration with the AS1411 aptamer and PEG, the M2D NCs were synthesized, showing phenomenal nucleus-targeted PDT properties. This innovative approach offers a novel strategy for designing a functional nanozyme that specially target subcellular organelles to enhance the modulation of drug resistance in tumor eradication.[76] A novel nanozyme structure of Fe@ZIF-8@GOx nanorods (NRs) was proposed by Li *et al.*, wherein the NRs were prepared *via* the iron mineralization during the growth of ZIF-8, followed by glucose oxidase (GOx) loading. The NRs can be efficiently internalized into cancer cells under an external magnetic field, thereby initiating a cascade catalysis reaction as follows: at the outset, GOx catalyzes intracellular glucose into $H_2O_2$, followed by NRs serving as a peroxidase-like nanozyme to produce hydroxyl radicals ($^{\bullet}OH$) from $H_2O_2$ under mild acidic condition in lysosomes at physiological temperature. Concurrently, the combination of glucose consumption and continuous generation of toxic ROS achieves severe damage to tumor cells through starvation therapy (Fig. 9A1).[78] Fe@ZIF-8 NPs exhibited a ferrimagnetism with a coercive field of 0.022 T and remnant magnetization of 3.15 A $m^2$ $kg^{-1}$. In contrast, ZIF-8 NPs had no magnetism at room temperature (Fig. 9A2). The cytotoxicity test of CCK-8 indicated that using Fe@ZIF-8@GOx+magnet almost eradicated the cancer cells *in vitro* (Fig. 9A3).

In a similar way, Fang *et al.* integrated a nanoscale Co-ferrocene MOFs (Co-Fc NMOF) with high Fenton reaction activity and GOx to construct a cascade enzymatic/Fenton catalytic platform termed as Co-Fc@GOx. In this system, Co-Fc NMOF not only served as a versatile and efficient carrier for GOx, but also showed exceptional Fenton effect, leading to the generation of highly toxic $^{\bullet}OH$ radicals. In TME, GOx delivered by Co-Fc NMOF catalyzes the conversion of endogenous glucose to gluconic acid and $H_2O_2$. The resulting intracellular acidity and on-site concentration of $H_2O_2$ favors the Fenton reaction of Co-Fc NMOF, leading to enhanced generation of ROS (Fig. 9B1 and B2). The finding obtained from both *in vitro* and *in vivo* experiments demonstrated that the cascade enzymatic/Fenton catalytic reaction triggered by the Co-Fc@GOx nanozyme exhibits remarkable anticancer properties (Fig. 9B2 and B3).[77]

### 4.7 Magnetic 2D COFs nanocomposites for multimodal antitumor

COFs are a newly-emerged 2D crystalline material that possess the similar framework structure of MOFs, thereby exhibiting tunable spatial arrangement and orderly accurate assembly pattern.[129] In addition to sharing the common advantages of other 2D NMs, COFs demonstrate intriguing reactive properties and favorable biocompatibility, attributed to their diverse organic structure. The covalent organic unit can be designed and synthesized as a structure sensitive to TME with a controllable degradation period, thereby easily collapsing under TME stimuli, further exerting flexible action on tumor eradication with high biocompatibility. In recent years, M2D COFs CNs have been extensively investigated, increasingly emerging as promising candidates for photo/magneto-active nanoagents in tumor combination therapy.[130–133] Zhao *et al.* proposed a nanocomposite termed $Fe_3O_4$@COF-BSA-FA for targeted drug delivery, consisting of magnetic $Fe_3O_4$ as the core and functionalized COFs loading into DOX as the shell, further modified

 

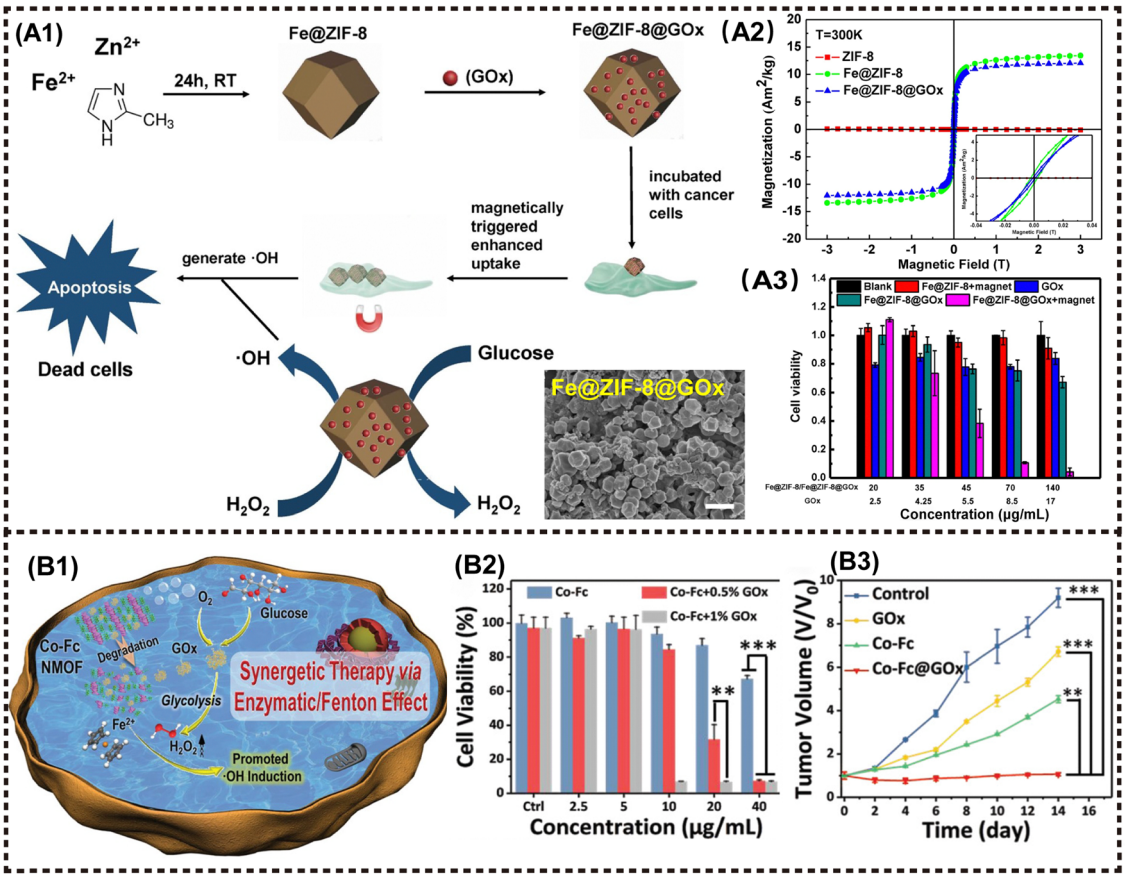


Fig. 9 Advanced magnetic 2D MOFs nanocomposites for cancer therapy and imaging. (A1) The fabrication procedure of Fe@ZIF-8@GOx NRs, and its combining PDT and starvation therapy for magnetically enhanced antitumor application. (A2) Magnetic hysteresis loop of ZIF-8 NPs, Fe@ZIF-8 NPs and Fe@ZIF-8@Gox NRs at 300 K. (A3) Relative viability of HeLa cells incubated with different materials. Reproduced with permission.[78] Copyright 2020, Elsevier. (B1) The synergetic therapy *via* Enzymatic/Fenton effect of Co-Fc@GOx as an antitumor platform. (B2) Cell viabilities of 4T1 tumor cells incubated with Co-Fc NMOF. (B3) Tumor volume variation of mice in the following 14 days. Reproduced with permission.[77] Copyright 2020, Wiley-ACH.

with bull serum albumin (BSA) and folic acid (FA) (Fig. 10A1). The tumor inhibition rate was observed to reach up to 80% (Fig. 10A3). More importantly, the π–π interaction between DOX and COFs provides a fluorescence resonance energy transfer (FRET) system, enabling the monitoring of drug release through changes in both UV absorption and fluorescence intensity.[81]

Cai *et al.* proposed a nanocomposite denoted as COFs-Au–$MnO_2$ for implementing the ROS catalysis reaction in TME, where Au NPs were grown on the surface using COFs as a template and then modified with a thin layer of $MnO_2$ before being coated with biocompatible hyaluronic acid (HA). Under hypoxic conditions in TME, COFs-Au–$MnO_2$ can react with overexpressed $H_2O_2$ to produce $O_2$, enhancing type II PDT. Au NPs can also decompose glucose to promote starvation therapy, while the resulting $H_2O_2$ benefits oxygen generation. Meanwhile, $MnO_2$ consumes GSH, thereby elevating the oxidative stress level. The released $Mn^{2+}$ can be utilized for $T_1$-MRI. *In vitro* and *in vivo* experiments demonstrated the strong tumor killing efficiency of this cascade cycle.[80] M2D COFs CNs can also serve as a versatile multimodal imaging agent. Feng *et al.* proposed the synthesis of $Fe_3O_4$@COF-DhaTph, a core–shell structured nanocomposite, through an *in situ* seed growth method (Fig. 10B1). This nanocomposite enabled dual-modal phototherapy with a single laser irradiation. More importantly, the high relaxation rate and excellent PTCE enable the expedient realization of tri-modal MR/PA/IR imaging-guided treatment (Fig. 10B2and B3). The combined phototherapy demonstrated the ability to kill cancer cells effectively *in vitro*, and suppress tumor growth with excellent biocompatibility *in vivo* (Fig. 10B4 and B5).[79]

### 4.8 Other magnetic 2D composites for multimodal antitumor

In addition to the aforementioned 2D NMs, numerous other newly emerging 2D NMs have been harnessed for the fabrication of advanced M2D NCs in biomedical applications, including boron nitride nanosheets (BNNSs), g-$C_3N_4$ nanosheets, 2D $FePSe_3$ nanosheets and so on.[101] 2D BNNSs with high NIR absorption properties are a promising PTT agent. Zhang *et al.* proposed a facile hydrothermal substitution method for the *in situ* formation of Pd NPs on the BNNSs surface, resulting in well-dispersed Pd@OH-BNNSs (Fig. 11A1).[82] Both Pd NPs and BNNSs exhibit high PTCE and wide-band NIR absorption. Moreover, the modification of Pd has been demonstrated to

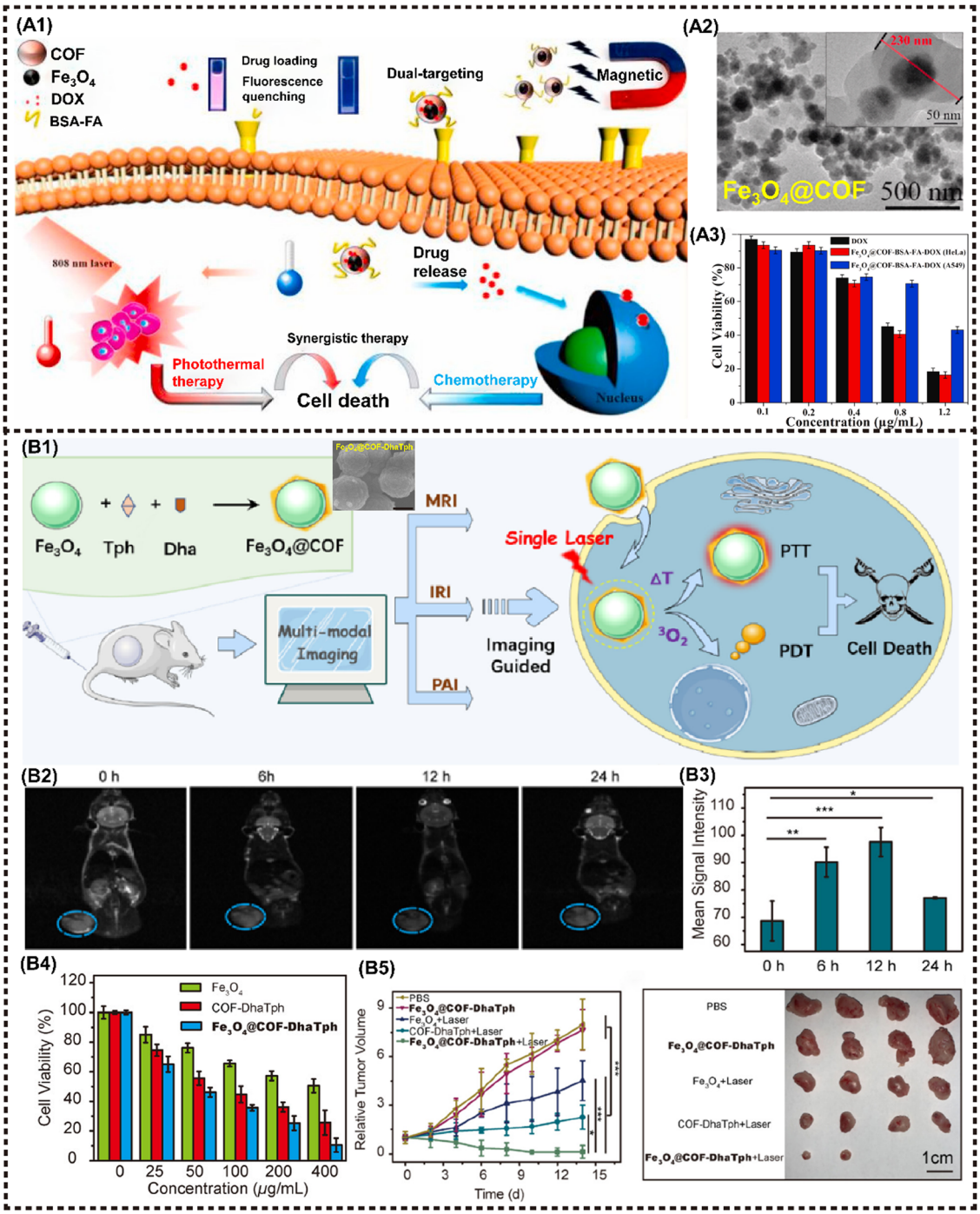


Fig. 10 Advanced magnetic 2D COFs nanocomposites for cancer therapy and imaging. (A) Schematic diagram for constructing the $Fe_3O_4$@COF-BSA-FA drug delivery system and PTT/chemotherapy synergistic treatment. Reproduced with permission.[81] Copyright 2021, Elsevier. (B) Schematic illustration of $Fe_3O_4$@COF-DhaTph as a multifunctional nanosystem for MR/PA/IR imaging-guided combined phototherapy upon single laser excitation. Reproduced with permission.[80] Copyright 2021, ACS.

prolong blood circulation, thereby allowing massive accumulation of MNMs at the targeted tumor site for enhanced PTT. Additionally, Pd@OH-BNNSs displayed heat-triggered drug release behavior, and the synergistic treatment significantly suppressed tumor growth within a mere two weeks (Fig. 11A2 and A3).

Graphitic-phase carbon nitride ($g\text{-}C_3N_4$)-based MNMs has attracted far-ranging attention due to the high photoluminescence quantum yield, facile fabrication, great biocompatibility, and low toxicity.[134] Ma *et al.* developed a mitochondria-targeting PDT nanoplatform that exhibits excellent $O_2$ catalytic production from $H_2O_2$ in cancer cells, utilizing $Fe^{III}$-doped 2D g-

 

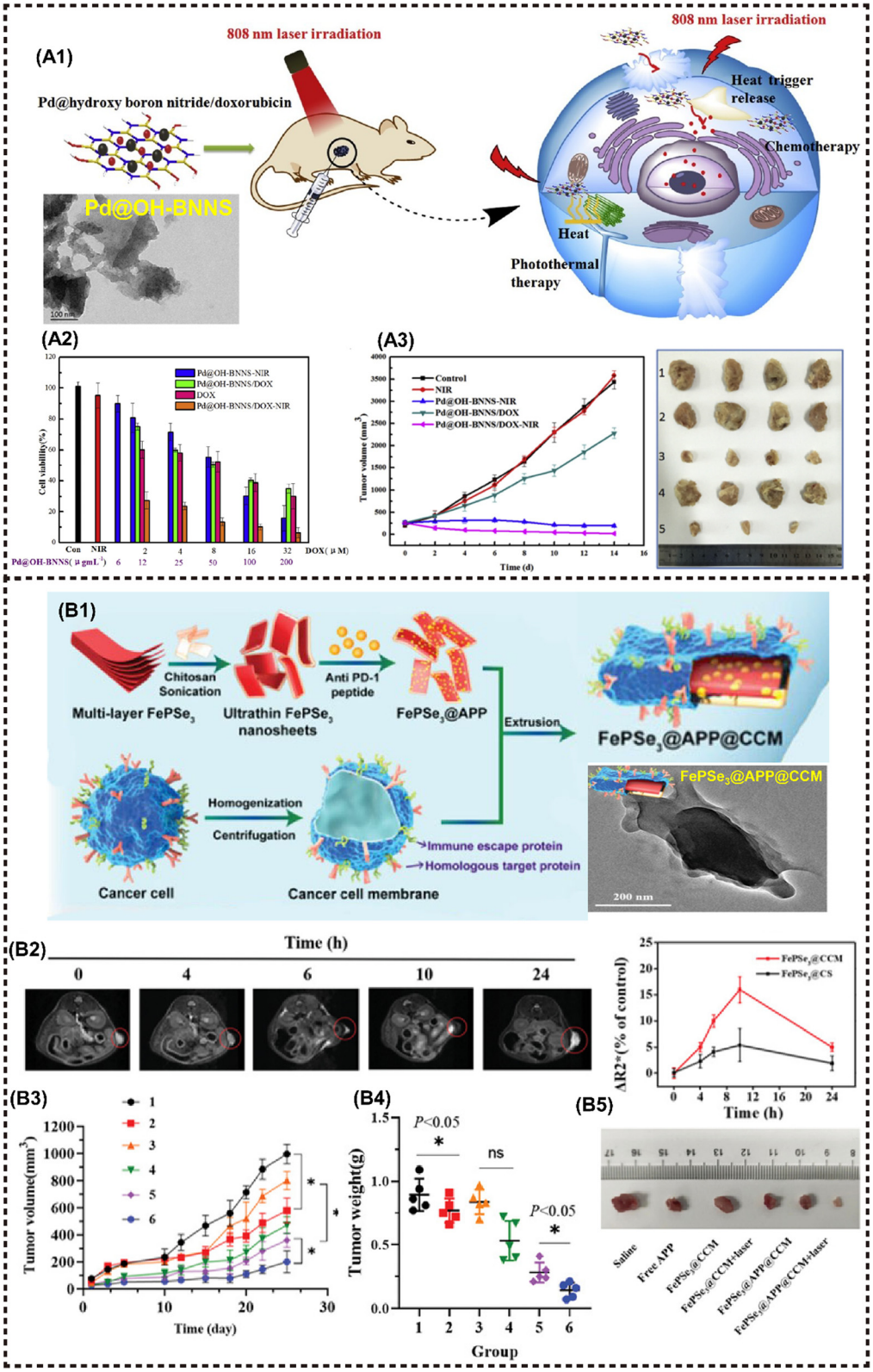


Fig. 11 Other magnetic 2D nanocomposites for cancer therapy and imaging. (A1) Schematic presentation for the synthesis of Pd@OH-BNNS/DOX and the PTT/chemotherapy synergistic antitumor mechanism. (A2) Viabilities of MCF-7 cells incubated with various materials. (A3) Tumor volumes of different groups during therapy (left) and tumor tissues (right). Reproduced with permission.[82] Copyright 2019, Elsevier. (B1) Schematic illustration for the preparation of FePSe$_3$@APP@CCM NSs. (B2) $T_2$-weighted MR images of FePSe$_3$@CCM NSs in the tumor site (left), and the $\Delta R^{2*}$ value in the tumor site after i.v. injection with FePSe$_3$@CCM NSs and FePSe3@CS NSs at different time intervals (right). (B3) Tumor growth curves and (B4) tumor weight plots of tumor-bearing mice from the different treatment groups (1: control; 2: free APP; 3: FePSe$_3$@CCM; 4: FePSe$_3$@CCM plus laser irradiation; 5: FePSe$_3$@APP@CCM; 6: FePSe$_3$@APP@CCM plus laser irradiation). (B5) Photographs of tumor tissues resected from mice after different treatment groups. Reproduced with permission.[83] Copyright 2021, Wiley-ACH.

$C_3N_4$ nanoholes. Moreover, this platform confers prominent $T_1$-MRI capability *in vivo*.[84] A metal phosphorous trichalcogenides ($MPX_3$)-based magnetic nanohybrid has been developed in recent years as an efficient PTT/CDT/MRI anti-cancer theranostic platform. For instance, Fang *et al.* developed a $FePSe_3$-based MNMs ($FePSe_3$@APP@CCM) functionalized with anti-PD-1 peptide (APP), which can serve as the MRI/PAI contrast agent and PTT/immunotherapeutic agent against CT26 cancer cells by targeting immune escape mechanisms (Fig. 11B1).[83] The functionalized 2D $FePSe_3$-based NSs exhibit an efficient tumor targeting ability because of the CCM decoration, and strong APP-related immunotherapy triggered by PTT, which can be monitored by precise MRI (Fig. 11B2). The multimodal imaging guided synergistic therapy significantly prolongs the lifespan of experimental mice (Fig. 11B3–B5).

# 5. Summary and perspectives

This review presents an overview of the recent advances in M2D NCs and their multimodal antitumor implementation. Advantages of the synergistic combination of 2D NMs and MNMs into M2D NCs are first discussed, followed by an introduction of the design and material fabrication of M2D NCs. Multimodal antitumor applications of M2D NCs, including 2D graphene and its derivatives, TMDs, transition metal carbides/nitrides/carbonitrides, BPs, LDHs, MOFs and COFs, are summarized and discussed. In particular, a detailed analysis is presented on the multimodal applications, including MHT, PTT, PDT, drug delivery, immunotherapy and multimodal imaging. Lastly, this review proposes the future development of such a research field with an emphasis on the scaling up of material fabrication, inherent structure-performance relationship, and elucidating the biodegradation mechanism. Additionally, it offers the capability to remotely modulate the structure disintegration and drug release in response to various external stimuli or TME conditions, holding great potential for achieving a more effective tumor treatment and facilitating the development of intelligent nanomedicine platforms, such as stimuli-responsive theranostic and cascade nanozyme catalytic reaction systems. Undoubtedly, M2D NCs have a great prospect for clinical translation in tumor treatment, while still facing some challenges and limitations that need to be tackled. Here, we make a comprehensive analysis of the challenges and clinical prospects associated with M2D NCs.

## 5.1 Challenges

The practical antitumor applications of M2D NCs in clinics is still currently encountering some challenges, with the primary concern being their controllable fabrication. The imperative for scalable application hinges on achieving production that is both controllable and repeatable. The attainment of M2D NCs characterized by high performance, uniform shape, customized size, and robust stability necessitates the development of meticulously designed material synthesis conditions. Upon transitioning from laboratory settings to semi-works plants, a re-exploration of the effects of temperature, pressure, reagent addition, gaseous atmosphere, and the selection of elements or functional molecules on the physiochemical properties of M2D NCs becomes paramount. Another challenge pertains to adhering to stringent quality standards in pharmaceutics. Analogous to conventional clinical drugs or materials, it is indispensable to standardize the dosage, administration regimen, contraindications, and precautions associated with the use of M2D NCs as a pharmaceutical agent. Prior to clinical implementation, comprehensive preclinical investigations must be conducted to assess the long-term safety, biodegradability, and potential toxicities linked to M2D NCs, ensuring their adequate safety for *in vivo* use. Potential bio-risks may arise not only from the toxic chemical solvents or reagents employed in the product fabrication, but also from the toxic degradation components or byproducts. The mitigation of these risks necessitates advanced green manufacturing approaches, substantial investment, and long-term tracking investigations. Lastly, the relationship between the structure of M2D NCs and their antitumor outcomes, as well as the biodegradation mechanism, remains unclear, and there is a lack of sophisticated measurements for precise prediction and systematic analysis. Despite significant efforts to comprehend the interaction between M2D NCs and TME, the intricate mutual effects are still unknown, warranting urgent and thorough investigation.

## 5.2 Opportunities and outlooks

Despite the numerous challenges facing M2D NCs and their early-stage clinical applications in antitumor treatment, notable progress has been made in the development of M2D NCs for multimodal antitumor therapy. Recent advancements in various emerging thoughts and technologies hold promise for addressing these challenges, thereby facilitating further clinical advancements.

The first imperative involves leveraging the advantages of artificial intelligence (AI)-guided material customization. AI, in its capacity, extends beyond merely screening material species and synthesis routes or predicting therapeutic performance. It significantly contributes to enhancing our comprehension of the interactions between M2D NCs and malignancy. This encompasses elucidating the targeting pathway, cellular uptake, intercellular transportation, and cumulative outcomes in tumor regions. For instance, machine learning (ML), as a subset of AI, discerns crucial information from extensive data regarding the structure and physicochemical properties of M2D NCs. ML not only refines the structure-performance relationships, but also predicts the potential decomposition and metabolic fates within the human body. The notable accuracy of ML models, surpassing that of other simulation methods, is a noteworthy attribute. Moreover, AI can guide each step in the development journey of M2D NCs – from material design and lab synthesis to *in vitro* or *in vivo* performance evaluation and large-scale manufacturing – resulting in an ultra-short research and development (R&D) cycle. Consequently, AI significantly enhances the efficiency of material design, reduces production

 

costs, mitigates utilization risks, and unequivocally accelerates the clinical translation of M2D NCs.

The second critical aspect underscores the advantages derived from the advancements in the in-depth understanding of tumorigenesis and metastasis pathology. The ongoing exploration of an expanding array of pathogenic factors and tumor biomarkers, such as diverse kinases, RNA molecules, and cellular signaling pathways, provides a foundation for potential intervention approaches at the cellular and molecular biology levels. This, in turn, catalyzes novel attempts through the utilization of M2D NCs, offering a promising avenue for the development of feasible tumor theranostic schemes. Furthermore, insights gleaned from the study of biological behaviors, encompassing immunoregulation, gene expression, pharmacokinetics, long-term biotoxicity, contribute to a nuanced understanding, promoting the rational design and administration of M2D NCs that are more aptly suited for clinical use in tumor treatment.

The third facet underscores the convenience derived from the widespread utilization of magnetic or optical theranostic devices and other technologies in clinical settings. Electric magnetic instruments and laser therapy apparatuses have become staple tools in clinical physiotherapy and rehabilitation, effectively alleviating inflammation, edema, muscle pain, and other injuries. Moreover, the integration of MRI and magnetic hyperthermia apparatus has proven successful in clinical tumor diagnostics and therapy. Leveraging the synergy of AI and electronics technology has led to the development of more intelligent magnetic and optical medical devices, enhancing precision and personalization in theranostic applications. Consequently, the proliferation of these advanced medical devices establishes a robust foundation for the widespread use of M2D NCs.

In conclusion, owing to their distinctive magnetic responsiveness and intelligent stimuli-response behaviors, including optical and immune modulation, coupled with the inherent biosecurity within the internal environment of the human body, M2D NCs present a promising clinical outlook. With increasing emphasis on controlled synthesis, functionalization, and a deeper comprehension of the mechanisms underlying multimodal antitumor therapy, it is anticipated that novel M2D NCs with tailored pharmaceutical properties will emerge. These advancements are expected to position M2D NCs as qualified multimodal antitumor nanomedicine in practical applications in the near future.

## Author contributions

Ying Yuan: investigation, writing – original draft. Bo Chen: conceptualization, resources, investigation, funding acquisition, writing – original draft. Luping Song: investigation. Xingxing An: investigation. Qinrui Zhang: investigation. Hao Lu: writing – review & editing. Chang Ming Li: supervision, writing – review & editing. Chunxian Guo: supervision, funding acquisition, writing – review & editing.

## Conflicts of interest

There are no conflicts of interest to declare.

## Acknowledgements

The authors are grateful for the financial support from National Natural Science Foundation of China (22108187), Natural Science Foundation for Excellent Youth Scholars of Jiangsu Science (BK20230073, BK20220118), the National Key Research and Development Program of China (2021YFA0910403), Jiangsu Laboratory of Biological and Chemical Sensing and Biochip, and Suzhou Foreign Academician Workstation (SWY2021002).

## References

1 Q. Gao, J. Feng, W. C. Liu, C. Y. Wen, Y. H. Wu, Q. Liao, L. Zou, X. B. Sui, T. Xie, J. M. Zhang and Y. C. Hu, *Adv. Drug Delivery Rev.*, 2022, **188**, 114445.
2 S. Y. Wu, F. G. Wu and X. Y. Chen, *Adv. Mater.*, 2022, **34**, 2109210.
3 D. Crosby, S. Bhatia, K. M. Brindle, L. M. Coussens, C. Dive, M. Emberton, S. Esener, R. C. Fitzgerald, S. S. Gambhir, P. Kuhn, T. R. Rebbeck and S. Balasubramanian, *Science*, 2022, **375**, 1244.
4 J. Liu, S. S. Liew, J. Wang and K. Y. Pu, *Adv. Mater.*, 2022, **34**, 2103790.
5 B. Faubert, A. Solmonson and R. J. DeBerardinis, *Science*, 2020, **368**, 152.
6 M. Kim, M. Panagiotakopoulou, C. Chen, S. B. Ruiz, K. Ganesh, T. Tammela and D. A. Heller, *Nat. Rev. Cancer*, 2023, **10**, 581–599.
7 Z. Wang, Q. Ye, S. Yu and B. Akhavan, *Adv. Healthcare Mater.*, 2023, **12**, 2300105.
8 Z. Pei, H. Lei and L. Cheng, *Chem. Soc. Rev.*, 2023, **52**, 2031–2081.
9 T. Fan, L. Yan, S. He, Q. Hong, F. Ai, S. He, T. Ji, X. Hu, E. Ha, B. Zhang, Z. Li, H. Zhang, X. Chen and J. Hu, *Chem. Soc. Rev.*, 2022, **51**, 7732–7751.
10 M. Wu, X. Niu, R. Zhang and Z. Ping Xu, *Adv. Drug Delivery Rev.*, 2022, **119**, 114360.
11 B. Gaihre, M. A. Potes, V. Serdiuk, M. Tilton, X. Liu and L. Lu, *Biomaterials*, 2022, **284**, 114360.
12 J. A. Carrasco, P. Congost-Escoin, M. Assebban and G. Abellán, *Chem. Soc. Rev.*, 2023, **52**, 1288–1330.
13 G. Li, X. Deng, P. Chen, X. Wang, J. Ma, F. Liu and S.-F. Yin, *Chem. Eng. J.*, 2022, **433**, 134505.
14 A. Ahmed, S. Sharma, B. Adak, M. M. Hossain, A. M. LaChance, S. Mukhopadhyay and L. Sun, *InfoMat*, 2022, **4**, e12295.
15 L. Song, B. Chen, Z. Qin, X. Liu, Z. Guo, H. Lou, H. Liu, W. Sun, C. Guo and C. Li, *Adv. Healthcare Mater.*, 2022, **11**, 2102298.

16 R. Ettlinger, U. Laechelt, R. Gref, P. Horcajada, T. Lammers, C. Serre, P. Couvreur, R. E. Morris and S. Wuttke, *Chem. Soc. Rev.*, 2022, **51**, 464–484.
17 J. Hu, J. Hu, W. Wu, Y. Qin, J. Fu, C. Liu, P. H. Seeberger and J. Yin, *Acta Biomater.*, 2022, **148**, 206–217.
18 X. Z. Qiuqiang Zhan, B. Wang, N. Li and S. He, *Prog. Electromagn. Res.*, 2019, **166**, 107–117.
19 S. D. Rawson, V. Bayram, S. A. McDonald, P. Yang, L. Courtois, Y. Guo, J. Xu, T. L. Burnett, S. Barg and P. J. Withers, *ACS Nano*, 2022, **16**, 1896–1908.
20 J. Liu, C. Zhao, W. R. Chen and B. Zhou, *Coord. Chem. Rev.*, 2022, **469**, 214654.
21 S. Rahimi, Y. Chen, M. Zareian, S. Pandit and I. Mijakovic, *Adv. Drug Delivery Rev.*, 2022, **189**, 114467.
22 W. Tao, X. Zhu, X. Yu, X. Zeng, Q. Xiao, X. Zhang, X. Ji, X. Wang, J. Shi, H. Zhang and L. Mei, *Adv. Mater.*, 2017, **29**, 1603276.
23 Z. Lei, W. Zhu, S. Xu, J. Ding, J. Wan and P. Wu, *ACS Appl. Mater. Interfaces*, 2016, **8**, 20900–20908.
24 S. Keshri and S. Biswas, *Prog. Biomater.*, 2022, **11**, 347–372.
25 J. Chen, Z. Zhou, S. Luo, G. Liu, J. Xiang and Z. Tian, *Biosens. Bioelectron.*, 2022, 217.
26 B. Chen, J. Sun, F. Fan, X. Zhang, Z. Qin, P. Wang, Y. Li, X. Zhang, F. Liu, Y. Liu, M. Ji and N. Gu, *Nanoscale*, 2018, **10**, 7369–7376.
27 B. Chen, Z. Guo, C. Guo, Y. Mao, Z. Qin, D. Ye, F. Zang, Z. Lou, Z. Zhang, M. Li, Y. Liu, M. Ji, J. Sun and N. Gu, *Nanoscale*, 2020, **12**, 5521–5532.
28 B. Chen, R. Zhang, H. Wu, M. Li, G. Zhou and M. Ji, *J. Drug Delivery Sci. Technol.*, 2020, **57**, 101677.
29 T. Dippong, E. A. Levei and O. Cadar, *Nanomaterials*, 2021, **11**, 11051227.
30 M. A. M. Tarkistani, V. Komalla and V. Kayser, *Nanomaterials*, 2021, **11**, 1227.
31 N. Gu, Z. Zhang and Y. Li, *Nano Res.*, 2021, **15**, 1–17.
32 B. Chen, J. Xing, M. Li, Y. Liu and M. Ji, *Colloids Surf., B*, 2020, **190**, 110896.
33 X. Meng, D. Li, L. Chen, H. He, Q. Wang, C. Hong, J. He, X. Gao, Y. Yang, B. Jiang, G. Nie, X. Yan, L. Gao and K. Fan, *ACS Nano*, 2021, **15**, 5735–5751.
34 P. Wang, S. Liu, M. Hu, H. Zhang, D. Duan, J. He, J. Hong, R. Lv, H. S. Choi, X. Yan and M. Liang, *Adv. Funct. Mater.*, 2020, **30**, 2000647.
35 X. Cai, L. Jiao, H. Yan, Y. Wu, W. Gu, D. Du, Y. Lin and C. Zhu, *Mater. Today*, 2021, **44**, 211–228.
36 J. Wu, X. Wang, Q. Wang, Z. Lou, S. Li, Y. Zhu, L. Qin and H. Wei, *Chem. Soc. Rev.*, 2019, **48**, 1004–1076.
37 S. R. Ali and M. De, *ACS Biomater. Sci. Eng.*, 2022, **8**, 2932–2942.
38 Q. Wu, G. Chen, K. Gong, J. Wang, X. Ge, X. Liu, S. Guo and F. Wang, *Matter*, 2019, **1**, 496–512.
39 K. Yang, L. Hu, X. Ma, S. Ye, L. Cheng, X. Shi, C. Li, Y. Li and Z. Liu, *Adv. Mater.*, 2012, **24**, 1868–1872.
40 K. Yang, L. Feng and Z. Liu, *Adv. Drug Delivery Rev.*, 2016, **105**, 228–241.
41 Y. Chen, Y. Wu, B. Sun, S. Liu and H. Liu, *Small*, 2017, **13**, 214415.
42 W. Chen, J. Ouyang, X. Yi, Y. Xu, C. Niu, W. Zhang, L. Wang, J. Sheng, L. Deng, Y. N. Liu and S. Guo, *Adv. Mater.*, 2017, **30**, 1703458.
43 S. Dang, Y. Mo, J. Zeng, Y. Xu, Z. Xie, H. Zhang, B. Zhang and G. Nie, *Nanophotonics*, 2022, **11**, 5061.
44 T. Liu, C. Wang, W. Cui, H. Gong, C. Liang, X. Shi, Z. Li, B. Sun and Z. Liu, *Nanoscale*, 2014, **6**, 11219–11225.
45 M. J. Molaei, *J. Drug Delivery Sci. Technol.*, 2021, **61**, 101830.
46 X. Ma, H. Tao, K. Yang, L. Feng, L. Cheng, X. Shi, Y. Li, L. Guo and Z. Liu, *Nano Res.*, 2012, **5**, 199–212.
47 Y. Chen, P. Xu, Z. Shu, M. Wu, L. Wang, S. Zhang, Y. Zheng, H. Chen, J. Wang, Y. Li and J. Shi, *Adv. Funct. Mater.*, 2014, **24**, 4386–4396.
48 X. Yao, X. Niu, K. Ma, P. Huang, J. Grothe, S. Kaskel and Y. Zhu, *Small*, 2017, **13**, 1602225.
49 F. Wo, R. Xu, Y. Shao, Z. Zhang, M. Chu, D. Shi and S. Liu, *Theranostics*, 2016, **6**, 485–500.
50 Z. Kiani Nejad, A. Akbar Khandar and M. Khatamian, *Int. J. Pharm.*, 2022, **628**, 122254.
51 J. Wu, M. Wang, Y. Pan, Y. Pang, Y. Tang, C. Song, J. Zhu, X. Zhang and Q. Huang, *RSC Adv.*, 2022, **12**, 23786–23795.
52 E. Seyyedi Zadeh, N. Ghanbari, Z. Salehi, S. Derakhti, G. Amoabediny, M. Akbari and M. Asadi Tokmedash, *Mater. Chem. Phys.*, 2023, **297**, 127336.
53 G. Yang, H. Gong, T. Liu, X. Sun, L. Cheng and Z. Liu, *Biomaterials*, 2015, **60**, 62–71.
54 L. Cheng, C. Yuan, S. Shen, X. Yi, H. Gong, K. Yang and Z. Liu, *ACS Nano*, 2015, **9**, 11090–11101.
55 J. Yu, W. Yin, X. Zheng, G. Tian, X. Zhang, T. Bao, X. Dong, Z. Wang, Z. Gu, X. Ma and Y. Zhao, *Theranostics*, 2015, **5**, 931–945.
56 T. Liu, S. Shi, C. Liang, S. Shen, L. Cheng, C. Wang, X. Song, S. Goel, T. E. Barnhart, W. Cai and Z. Liu, *ACS Nano*, 2015, **9**, 950–960.
57 B. Liu, C. Li, G. Chen, B. Liu, X. Deng, Y. Wei, J. Xia, B. Xing, P. Ma and J. Lin, *Adv. Sci.*, 2017, **4**, 1600540.
58 C. Dai, H. Lin, G. Xu, Z. Liu, R. Wu and Y. Chen, *Chem. Mater.*, 2017, **29**, 8637–8652.
59 C. Dai, Y. Chen, X. Jing, L. Xiang, D. Yang, H. Lin, Z. Liu, X. Han and R. Wu, *ACS Nano*, 2017, **11**, 12696–12712.
60 Z. Liu, M. Zhao, H. Lin, C. Dai, C. Ren, S. Zhang, W. Peng and Y. Chen, *J. Mater. Chem. B*, 2018, **6**, 3541–3548.
61 Z. Liu, H. Lin, M. Zhao, C. Dai, S. Zhang, W. Peng and Y. Chen, *Theranostics*, 2018, **8**, 1648–1664.
62 M. Darroudi, S. Elnaz Nazari, M. Karimzadeh, F. Asgharzadeh, N. Khalili-Tanha, S. Z. Asghari, S. Ranjbari, F. Babaei, M. Rezayi and M. Khazaei, *Front. Bioeng. Biotechnol.*, 2023, **11**, 1097631.
63 Y. Wu, X. Song, W. Xu, K. Y. Sun, Z. Wang, Z. Lv, Y. Wang, Y. Wang, W. Zhong, J. Wei, H. L. Cai and X. Wu, *Small*, 2021, **17**, e2101705.
64 D. Yang, G. Yang, P. Yang, R. Lv, S. Gai, C. Li, F. He and J. Lin, *Adv. Funct. Mater.*, 2017, **27**, 1700371.
65 J. Liu, P. Du, T. Liu, B. J. Cordova Wong, W. Wang, H. Ju and J. Lei, *Biomaterials*, 2019, **192**, 179–188.

 

66 Q. Zhang, W. Wang, M. Zhang, F. Wu, T. Zheng, B. Sheng, Y. Liu, J. Shen, N. Zhou and Y. Sun, *Chem. Eng. J.*, 2020, **391**, 123525.
67 Y. Su, X. Zhang, L. Lei, B. Liu, S. Wu and J. Shen, *ACS Appl. Mater. Interfaces*, 2021, **13**, 12960–12971.
68 M. Zhang, W. Wang, F. Wu, K. Graveran, J. Zhang and C. Wu, *Chem. – Eur. J.*, 2018, **24**, 12890–12901.
69 L. Wang, H. Xing, S. Zhang, Q. Ren, L. Pan, K. Zhang, W. Bu, X. Zheng, L. Zhou, W. Peng, Y. Hua and J. Shi, *Biomaterials*, 2013, **34**, 3390–3401.
70 B. Li, Z. Gu, N. Kurniawan, W. Chen and Z. P. Xu, *Adv. Mater.*, 2017, **29**, 1700373.
71 G. Huang, K. L. Zhang, S. Chen, S. H. Li, L. L. Wang, L. P. Wang, R. Liu, J. Gao and H. H. Yang, *J. Mater. Chem. B*, 2017, **5**, 3629–3633.
72 H. Zuo, W. Chen, B. Li, K. Xu, H. Cooper, Z. Gu and Z. P. Xu, *Chemistry*, 2017, **23**, 14299–14306.
73 M. J. Molaei, *J. Cryst. Growth*, 2023, **611**, 127186.
74 Z. Liu, X. Wang, C. Zhang, K. Lin, J. Yang, Y. Zhang, J. Hao and F. Tian, *Int. J. Biol. Macromol.*, 2024, **256**, 128385.
75 D. Yang, G. Yang, S. Gai, F. He, G. An, Y. Dai, R. Lv and P. Yang, *Nanoscale*, 2015, **7**, 19568–19578.
76 X. Zeng, S. Yan, P. Chen, W. Du and B.-F. Liu, *Nano Res.*, 2020, **13**, 1527–1535.
77 C. Fang, Z. Deng, G. Cao, Q. Chu, Y. Wu, X. Li, X. Peng and G. Han, *Adv. Funct. Mater.*, 2020, **30**, 1910085.
78 J. Li, T. Li, D. Gorin, Y. Kotelevtsev, Z. Mao and W. Tong, *Colloids Surf., A*, 2020, **601**, 124900.
79 J. Feng, W. Ren, J. Gao, F. Li, F. Kong, B. Yao and Y. Dong, *ACS Appl. Mater. Interfaces*, 2021, **13**, 17243–17254.
80 L. Cai, C. Hu, S. Liu, Y. Zhou, M. Pang and J. Lin, *Sci. China Mater.*, 2020, **64**, 488–497.
81 K. Zhao, P. Gong, J. Huang, Y. Huang, D. Wang, J. Peng, D. Shen, X. Zheng, J. You and Z. Liu, *Microporous Mesoporous Mater.*, 2021, **311**, 110713.
82 Y. Zhang, R. Guo, D. Wang, X. Sun and Z. Xu, *Colloids Surf., B*, 2019, **176**, 300–308.
83 X. Fang, X. Wu, Z. Li, L. Jiang, W. S. Lo, G. Chen, Y. Gu and W. T. Wong, *Adv. Sci.*, 2021, **8**, 2003041.
84 Z. Ma, M. Zhang, X. Jia, J. Bai, Y. Ruan, C. Wang, X. Sun and X. Jiang, *Small*, 2016, **12**, 5477–5487.
85 R. Tietze, J. Zaloga, H. Unterweger, S. Lyer, R. P. Friedrich, C. Janko, M. Pottler, S. Durr and C. Alexiou, *Biochem. Biophys. Res. Commun.*, 2015, **468**, 463–470.
86 S. Dash, T. Das, P. Patel, P. K. Panda, M. Suar and S. K. Verma, *J. Nanobiotechnol.*, 2022, **20**, 393.
87 I. Blazkova, H. V. Nguyen, S. Dostalova, P. Kopel, M. Stanisavljevic, M. Vaculovicova, M. Stiborova, T. Eckschlager, R. Kizek and V. Adam, *Int. J. Mol. Sci.*, 2013, **14**, 13391–13402.
88 R. Ahmad, Z. Ali, X. Mou, J. Wang, H. Yi and N. He, *J. Nanosci. Nanotechnol.*, 2016, **16**, 9393–9403.
89 E. A. Périgo, B. Weidenfeller, P. Kollár and J. Füzer, *Appl. Phys. Rev.*, 2018, **5**, 031301.
90 A. A. Maria Moros, G. Stepien, F. Fabozzi, V. Marchesano, A. Castaldi, A. Tino, J. M. de la Fuente and C. Tortiglione, *Nanomedicine*, 2015, **10**, 14.
91 Y. Qu, B. Chu, X. Wei, M. Lei, D. Hu, R. Zha, L. Zhong, M. Wang, F. Wang and Z. Qian, *J. Controlled Release*, 2019, **296**, 93–106.
92 Y. Zhang, W. Song, Y. Lu, Y. Xu, C. Wang, D. G. Yu and I. Kim, *Biomolecules*, 2022, **12**, 636.
93 L. Z. Bai, D. L. Zhao, Y. Xu, J. M. Zhang, Y. L. Gao, L. Y. Zhao and J. T. Tang, *Mater. Lett.*, 2012, **68**, 399–401.
94 W. Feng, P. Long, Y. Feng and Y. Li, *Adv. Sci.*, 2016, **3**, 1500413.
95 Y. Fujii, T. Ogiwara, H. Kato, Y. Hanaoka, R. F. Hardian, T. Goto, K. Hongo and T. Horiuchi, *Neurol. Med. Chir.*, 2022, **62**, 328–335.
96 Z. Qi, L. Li and Z. P. Xu, *Particuology*, 2022, **64**, 121–133.
97 Y. Hao, L. Wang, B. Zhang, D. Li, D. Meng, J. Shi, H. Zhang, Z. Zhang and Y. Zhang, *Int. J. Nanomed.*, 2016, **2016**, 1759–1778.
98 P. Kumbhakar, C. Chowde Gowda, P. L. Mahapatra, M. Mukherjee, K. D. Malviya, M. Chaker, A. Chandra, B. Lahiri, P. M. Ajayan, D. Jariwala, A. Singh and C. S. Tiwary, *Mater. Today*, 2021, **45**, 142–168.
99 A. Szuplewska, D. Kulpinska, A. Dybko, M. Chudy, A. M. Jastrzebska, A. Olszyna and Z. Brzozka, *Trends Biotechnol.*, 2020, **38**, 264–279.
100 R. Gusain, N. Kumar and S. S. Ray, *Coord. Chem. Rev.*, 2020, **405**, 213111.
101 L. Cheng, X. Wang, F. Gong, T. Liu and Z. Liu, *Adv. Mater.*, 2020, **32**, e1902333.
102 H. Hwang, H. Kim and J. Cho, *Nano Lett.*, 2011, **11**, 4826–4830.
103 C. Tan and H. Zhang, *Nat. Commun.*, 2015, **6**, 7873.
104 W. Zheng, Z. Li, G. Lu, T. Yang, M. Li, C. Xu and R. Wang, *Chem. Eng. J.*, 2023, **451**, 138581.
105 Z. Cai, B. Liu, X. Zou and H. M. Cheng, *Chem. Rev.*, 2018, **118**, 6091–6133.
106 Q. Lu, J. Wang, Y. Miao, Y. Guo, G. Wang, J. Dong, M. Zhao and H. Wang, *Chem. Eng. J.*, 2022, **450**, 138439.
107 J. N. Coleman, M. Lotya, A. O'Neill, S. D. Bergin, P. J. King, U. Khan, K. Young, A. Gaucher, S. De, R. J. Smith, I. V. Shvets, S. K. Arora, G. Stanton, H.-Y. Kim, K. Lee, G. T. Kim, G. S. Duesberg, T. Hallam, J. J. Boland, J. J. Wang, J. F. Donegan, J. C. Grunlan, G. Moriarty, A. Shmeliov, R. J. Nicholls, J. M. Perkins, E. M. Grieveson, K. Theuwissen, D. W. McComb, P. D. Nellist and V. Nicolosi, *Science*, 2011, **331**, 568–571.
108 F. H. Sani, M. Pourfallah and M. Gholinia, *Case Stud. Therm. Eng.*, 2022, **30**, 101760.
109 Q. H. Wang, K. Kalantar-Zadeh, A. Kis, J. N. Coleman and M. S. Strano, *Nat. Nanotechnol.*, 2012, **7**, 699–712.
110 M. A. Haghighat Bayan, Y. J. Dias, C. Rinoldi, P. Nakielski, D. Rybak, Y. B. Truong, A. L. Yarin and F. Pierini, *J. Polym. Sci.*, 2023, **61**, 521–533.
111 M. Rafiq, S.-u Rather, T. U. Wani, A. H. Rather, R. S. Khan, A. E. Khan, I. Hamid, H. A. Khan, A. S. Alhomida and F. A. Sheikh, *Chin. Chem. Lett.*, 2023, **34**, 108463.
112 J. Kudr, Y. Haddad, L. Richtera, Z. Heger, M. Cernak, V. Adam and O. Zitka, *Nanomaterials*, 2017, **7**, 243.

113 W. Wu, Z. Wu, T. Yu, C. Jiang and W. S. Kim, *Sci. Technol. Adv. Mater.*, 2015, **16**, 023501.
114 J. Shao, H. Xie, H. Huang, Z. Li, Z. Sun, Y. Xu, Q. Xiao, X. F. Yu, Y. Zhao, H. Zhang, H. Wang and P. K. Chu, *Nat. Commun.*, 2016, **7**, 12967.
115 L. Cheng, S. Shen, S. Shi, Y. Yi, X. Wang, G. Song, K. Yang, G. Liu, T. E. Barnhart, W. Cai and Z. Liu, *Adv. Funct. Mater.*, 2016, **26**, 2185–2197.
116 Y. Chen, Z. Fan, Z. Zhang, W. Niu, C. Li, N. Yang, B. Chen and H. Zhang, *Chem. Rev.*, 2018, **118**, 6409–6455.
117 A. K. Swain, L. Pradhan and D. Bahadur, *ACS Appl. Mater. Interfaces*, 2015, **7**, 8013–8022.
118 S. Hatamie, M. M. Ahadian, M. A. Ghiass, A. Iraji Zad, R. Saber, B. Parseh, M. A. Oghabian and S. Shanehsazzadeh, *Colloids Surf., B*, 2016, **146**, 271–279.
119 S. Y. Yin, G. Song, Y. Yang, Y. Zhao, P. Wang, L. Zhu, X. Yin and X. B. Zhang, *Adv. Funct. Mater.*, 2019, **29**, 1901417.
120 T. Gong, X. Wang, H. Zhu, C. Wen, Q. Ma, X. Li, M. Li, R. Guo and W. Liang, *RSC Adv.*, 2023, **13**, 12609–12617.
121 M. Naguib, M. Kurtoglu, V. Presser, J. Lu, J. Niu, M. Heon, L. Hultman, Y. Gogotsi and M. W. Barsoum, *Adv. Mater.*, 2011, **23**, 4248–4253.
122 H. Lin, X. Wang, L. Yu, Y. Chen and J. Shi, *Nano Lett.*, 2017, **17**, 384–391.
123 X. Han, J. Huang, H. Lin, Z. Wang, P. Li and Y. Chen, *Adv. Healthcare Mater.*, 2018, **7**, e1701394.
124 H. Lin, Y. Wang, S. Gao, Y. Chen and J. Shi, *Adv. Mater.*, 2018, **30**, 1703284.
125 X. Yang, G. Liu, Y. Shi, W. Huang, J. Shao and X. Dong, *Nanotechnology*, 2018, **29**, 222001.
126 X. F. Zhao, W. Y. Wang, X. D. Li, S. P. Li and F. G. Song, *Mater. Sci. Eng.*, 2018, **89**, 422–428.
127 M. S. Usman, M. Z. Hussein, S. Fakurazi and F. F. Ahmad Saad, *Chem. Cent. J.*, 2017, **11**, s13065.
128 J. Wu, A. Deng, W. Jiang, R. Tian and Y. Shen, *Biomater. Adv.*, 2017, **71**, 132–140.
129 D. D. Medina, T. Sick and T. Bein, *Adv. Energy Mater.*, 2017, **7**, 1700387.
130 F. Yang, C. Li, C. Xu, J. Kan, B. Tian, H. Qu, Y. Guo, Y. Geng and Y. Dong, *Chem. Commun.*, 2022, **58**, 1530–1533.
131 S. Wan, J. Guo, J. Kim, H. Ihee and D. Jiang, *Angew. Chem., Int. Ed.*, 2008, **47**, 8826–8830.
132 G. Kumar, M. Singh, R. Goswami and S. Neogi, *ACS Appl. Mater. Interfaces*, 2020, **12**, 48642–48653.
133 M. Matsumoto, L. Valentino, G. M. Stiehl, H. B. Balch, A. R. Corcos, F. Wang, D. C. Ralph, B. J. Mariñas and W. R. Dichtel, *Chem*, 2018, **4**, 308–317.
134 L. S. Lin, Z. X. Cong, J. Li, K. M. Ke, S. S. Guo, H. H. Yang and G. N. Chen, *J. Mater. Chem. B*, 2014, **2**, 1031–1037.

 